Pergamon

Neural Networks

Neural Networks 11 (1998) 189–208

A neural network model for the development of simple and complex cell receptive fields within cortical maps of orientation and ocular dominance[1]

Steven J. Olson[2], Stephen Grossberg*[3]

Department of Cognitive and Neural Systems and Center for Adaptive Systems, Boston University, 677 Beacon Street, Boston, MA 02215, USA

Received 9 December 1996; accepted 26 November 1997

Abstract

Prenatal development of the primary visual cortex leads to simple cells with spatially distinct and oriented ON and OFF subregions. These simple cells are organized into spatial maps of orientation and ocular dominance that exhibit singularities, fractures, and linear zones. On a finer spatial scale, simple cells occur that are sensitive to similar orientations but opposite contrast polarities, and exhibit both even-symmetric and odd-symmetric receptive fields. Pooling of outputs from oppositely polarized simple cells leads to complex cells that respond to both contrast polarities. A neural network model is described which simulates how simple and complex cells self-organize starting from unsegregated and unoriented geniculocortical inputs during prenatal development. Neighboring simple cells that are sensitive to opposite contrast polarities develop from a combination of spatially short-range inhibition and high-gain recurrent habituative excitation between cells that obey membrane equations. Habituation, or depression, of synapses controls reset of cell activations both through enhanced ON responses and OFF antagonistic rebounds. Orientation and ocular dominance maps form when high-gain medium-range recurrent excitation and long-range inhibition interact with the short-range mechanisms. The resulting structure clarifies how simple and complex cells contribute to perceptual processes such as texture segregation and perceptual grouping.

Keywords: Development; Self-organization; Visual cortex; V1; Lateral geniculate nucleus; Simple cell; Complex cell; Cortical map; Ocular dominance column; Orientation column; Orientation tuning; Neural network

1. Introduction: development of cortical orientation and ocular dominance maps with oppositely polarized simple cells

Development of the primary visual cortex prior to visual experience produces orientationally tuned cortical neurons, classifiable according to the criteria of Hubel and Wiesel (1962) as either simple or complex; after several weeks of visual experience these cortical cells evolve adult responsivity (DeAngelis et al., 1993; Ghose et al., 1994; Hubel and Wiesel, 1974). The prenatal segregation of geniculocortical afferents into ocular dominance columns also occurs independently of visual experience (Horton and Hocking, 1996). Monocular, but not binocular, deprivation during the first few weeks of visual experience can lead to drastic changes in the arrangement of ocular dominance patches (Hubel et al., 1977), but these changes may be blocked by the elimination of neural activity (Stryker and Harris, 1986), suggesting that an activity-dependent process is responsible for the development of ocular dominance.

Adult cortical cells are arranged into vertical columns with similar orientation tuning and ocular dominance, and these columns are arranged into smoothly changing two-dimensional maps of orientation and ocular dominance (Hubel and Wiesel, 1962, 1963, 1968). The cortical map of orientation is arranged in swirling patterns around orientation centers in both cats (Bonhoeffer and Grinvald, 1991; Grinvald et al., 1994) and monkeys (Blasdel, 1992b; Blasdel and Salama, 1986), but the patchy pattern of ocular dominance in cats (Anderson et al., 1988; LeVay et al., 1978; Löwel and Singer, 1987; Löwel et al., 1988) differs somewhat from the stripe-like pattern in monkeys (Blasdel, 1992a, b; Hubel et al., 1977, 1978; LeVay et al., 1975, 1985; Obermayer and Blasdel, 1993). In both species these patterns are evident at a spatial scale of about 1 mm.

* Requests for reprints should be sent to Professor Stephen Grossberg. Tel.: +1 617 353 7858; Fax: +1 617 353 7755; e-mail: steve@cns.bu.edu

[1] Technical Report CAS/CNS-TR-96-021.

[2] Supported in part by the Air Force Office of Scientific Research (AFOSR F49620-92-J-0334), British Petroleum (BP 89A-1204), the National Science Foundation (NSF IRI-90-24877), and the Office of Naval Research (ONR N00014-91-J-4100).

[3] Supported in part by the Defense Advanced Research Projects Agency and the Office of Naval Research (ONR N00014-91-J-4100 and ONR N00014-95-1-0409).

0893–6080/98/$19.00
PII S0893-6080(98)00003-3

At a much smaller spatial scale, nearby cortical simple cells tend to exhibit opposite spatial phase (Pollen and Ronner, 1981), and these cells may be connected by functionally inhibitory connections (DeAngelis et al., 1991; Liu et al., 1992; Palmer and Davis, 1981). The proposed arrangement of simple cells with complementary ON and OFF zones into mutually inhibitory pairs helps to explain the source of local intracortical inhibition which provides functional antagonism between ON and OFF zones in simple cell receptive fields (Hubel and Wiesel, 1962). This complementary representation also helps to explain the robust expression of orientation tuning following blockade of ON retinal ganglion cells by the application of APB (Schiller, 1982). These facts are summarized well by models in which ON and OFF geniculate afferents synapse onto pairs of mutually inhibitory simple cells (e.g. Gove et al., 1995; Shulz et al., 1993).

Complex cells also respond to oriented stimuli, but do not have well-segregated ON and OFF receptive field subregions. Complex cells are found in almost every layer of V1 (Gilbert, 1977), and are important components of cortical models of visual perception (e.g. Grossberg and Mingolla, 1985a, b). Several models of how individual complex cells achieve their orientation tuning without segregated ON and OFF regions have been described, each of which pools simple cell responses with differing spatial phases at a single complex cell (Emerson et al., 1992; Gove et al., 1995; Grossberg and Mingolla, 1985a, b; Jacobson et al., 1993; Spitzer and Hochstein, 1985).

2. Some previous map development models

A number of theoretical models demonstrate how simple cell response characteristics and global maps can be simultaneously self-organized by local processes. One of the earliest models showed how a neural network with weights modified by an associative learning rule can produce orientation tuning when presented with oriented inputs (Grossberg, 1976a, c; von der Malsburg, 1973). Linsker (1986a, b, c) subsequently demonstrated the self-organization of orientation tuning without oriented inputs. Other modeling work has shown how ocular dominance maps can arise from uncorrelated inputs (Kohonen, 1982, 1989; Miller et al., 1989; Rojer and Schwartz, 1989, 1990; Swindale, 1980), how maps of orientation can form (Swindale, 1982), how maps of orientation and ocular dominance may develop simultaneously (Durbin and Mitchison, 1990; Obermayer et al., 1990, 1992; Sirosh and Miikkulainen, 1994; Swindale, 1992), and how the development of orientationally tuned simple cells and their arrangement into cortical maps may progress synchronously (Miller, 1992, 1994). Each of these models computes its maps with somewhat different equations. Some models, for example, focus on the learning that alters neural connections without modeling the dynamics of the cells themselves; e.g. Miller (1992, 1994). The fact that all of these models realize three computational principles (Grossberg and Olson, 1994)—a source of noise, a band pass filter, and normalization across all feature dimensions—clarifies what all these different models have in common from a computational viewpoint. These three factors are sufficient to generate cortical maps which exhibit the singularities, fractures, and linear zones that are found in vivo (Blasdel, 1992a, b).

3. Self-organizing cortical maps and the triple-o map

A neural network model is described here that builds upon these earlier developmental models. The model was first presented in Olson and Grossberg (1996). This model demonstrates the self-organization of cortical maps of ocular dominance and orientation, while simultaneously developing neighboring orientationally tuned simple cells that are sensitive to opposite contrast polarities, and that exhibit either even-symmetric or odd-symmetric receptive fields. As shown below, these paired simple cells provide a natural explanation for such facts as how subcortical application of APB influences cortical orientation tuning and how cortical complex cells come to pool signals from oppositely polarized simple cells within a developing cortical map.

This model is generically called a self-organizing cortical map (SOCM). In order to distinguish this SOCM from previous ones, it may be called a triple-o map model after its ability to self-organize orientation, ocular dominance, and opponent contrast cells in a map. Previous models, which develop one or two of the first properties, are thus single-o or double-o map models.

In order to achieve these results, the dynamics of both cortical cells and their intercellular interactions need to be explicitly modeled. In particular, the model starts with arrays of spatially contiguous opponent cortical cells for which offset of activity in one cell (or cell population) of a pair can lead to a transient antagonistic rebound of activity in the opponent cell (or cell population) of the pair. When embedded in a model whose dynamics realize the three computational properties listed above, these opponent cells develop into simple cells with similar orientation tuning but sensitivity to opposite contrast polarities.

As sketched in Fig. 1, the model also needs to simulate the processing performed at earlier stages in the visual pathway, most notably the relevant properties of the LGN (Schiller, 1992). Retinal signals from the two eyes project forward to ON and OFF cells in the LGN. ON and OFF geniculate inputs from both eyes converge onto each cortical simple cell via adaptive pathways. Driven by an activity-dependent associative learning rule, segregation of these geniculocortical connections is responsible for the development of orientation tuning in the model.

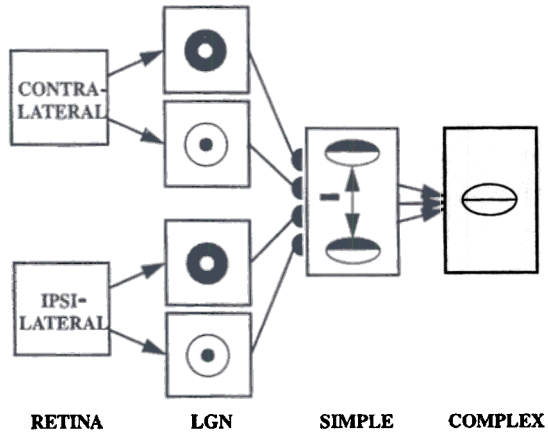

Fig. 1. Model overview: inputs to the two eyes project forward to ON and OFF cells in the LGN. ON and OFF cells from both eyes converge on cortical simple cells, which are arranged into mutually inhibitory pairs. The simple cells in turn project forward to complex cells. Model complex cells thus derive their orientation from the underlying simple cells.

3.1. LGN preprocessing

The relevant section of the visual field is represented by a two-dimensional array of intensity values, L^+, ranging between 0 and 1. Each of the values of this image corresponds roughly to the net photoreceptor activity within a small patch of foveal retina. Neural responses in the retina and in the LGN may be divided into two main groups: ON (+) cells and OFF (−) cells. Processing in the LGN is thus broken into two complementary streams corresponding to the representation by ON and OFF LGN cells of the pattern of light on the retina. The activity in each of the model ON cells (N^+) obeys membrane, or shunting, equations (Grossberg, 1973; Hodgkin and Huxley, 1952) with feed-forward on-center, off-surround interactions (with positional indices suppressed):

$$\frac{dN^+}{dt} = -\beta N^+ + (1-N^+)[\alpha_1 G(\sigma_1) * L^+] - (1+N^+)[\alpha_2 G(\sigma_2) * L^+]. \quad (1)$$

Two-dimensional spatial convolution is indicated by the '$*$' operator, and the array $G(\sigma)$ is a two-dimensional Gaussian with its peak at the center of the array at (i_0,j_0) as defined by

$$G(\sigma,i,j) = e^{-\frac{(i-i_0)^2+(j-j_0)^2}{\sigma^2}}. \quad (2)$$

The convolution operator shifts the center of the Gaussian in the usual way. Without the excitatory or inhibitory inputs, the passive decay term, $-\beta N^+$, causes the activity of each cell to exponentially decay towards 0. Sensitivity to excitatory inputs $\alpha_1 G(\sigma_1)*L^+$ decreases as the cell's activity level approaches 1 according to the term $(1-N^+)$, just as sensitivity to inhibitory inputs $\alpha_2 G(\sigma_2)*L^+$ decreases as the activity approaches -1 according to the term $(1+N^+)$. The behavior of this equation models neural hyperpolarization and depolarization in response to conductance changes. Activity in each model OFF cell (N^-) responds to the complement of the input image

$$L^-(j,k) = 1 - L^+(j,k) \quad (3)$$

according to

$$\frac{dN^-}{dt} = -\beta N^- + (1-N^-)[\varepsilon_1 G(\sigma_1) * L^- - (1+N^-)[\alpha_2 G(\sigma_2) * L^- \quad (4)$$

At steady state, the activity of the LGN cells becomes

$$N^+ = \frac{[\alpha_1 G(\sigma_1) - \alpha_2 G(\sigma_2)] * L^+}{\beta + [\alpha_1 G(\sigma_1) + \alpha_2 G(\sigma_2)] * L^+} \quad (5)$$

and

$$N^- = \frac{[\alpha_1 G(\sigma_1) - \alpha_2 G(\sigma_2)] * L^-}{\beta + [\alpha_1 G(\sigma_1) + \alpha_2 G(\sigma_2)] * L^-}. \quad (6)$$

The amplitudes of the two Gaussian kernels, $G(\sigma_1)$ and $G(\sigma_2)$, in the above convolutions are scaled by α_1 and α_2 so that the volumes under the two surfaces are equal to 1.0. In discrete form:

$$\alpha_1 \sum_{j,k} G(\sigma_1)(j,k) = \alpha_2 \sum_{j,k} G(\sigma_2)(j,k) = 1.0. \quad (7)$$

Eqs. (5) and (6) ensure that activity in the LGN field is locally correlated: local correlations in the LGN drive the development of local correlations in the receptive fields of downstream cortical simple cells. Changing the size of the two kernels by changing σ_1 and σ_2 alters the extents of the on-center/off-surround processing realized by Eqs. (5) and (6) and results in a corresponding change to the typical size of simple cell subfields that the model will produce.

Cells in the LGN do not respond at a constant firing frequency to constant patterns of light entering the retina. Rather, in response to activating stimuli, LGN cells quickly achieve a high firing rate which then decays over time (Cleland et al., 1971). Neither the exact shape of the response curve nor the precise timing of the habituation is important for the purposes of these simulations, but time dependence of model LGN cell responses enables the model to respond robustly to new inputs (see below). This habituative property is implemented by multiplying the maximal response of each geniculate cell, N^+ or N^-, by a Gaussian function of time since the start of the last pattern presentation, t_1:

$$\lambda(t) = e^{-\frac{(t-t_1)^2}{\sigma_t^2}}. \quad (8)$$

Utilizing such a function, rather than explicitly modeling frequency-dependent habituative LGN dynamics, helps to reduce the computational load which, as noted below, is considerable. More realistic frequency-dependent habituative processes in the cortex are dynamically modeled using differential equations.

3.2. Weighted geniculocortical connections

Each model simple cell (or cell population) $x_i(j,k)$ receives direct connections from only a subset of LGN ON and OFF cells, as shown in Fig. 2. These signals, $s^+(l,m)$ and $s^-(l,m)$, are copied from a circular region of diameter n_1 of the LGN activity patterns, $N^+(u,v)$ or $N^-(u,v)$, shifted downwards with increasing l and to the right with increasing values of m.

Each simple cell $x_i(j,k)$ has a separate set of synaptic weights $w^+_{ijk}(l,m)$ and $w^-_{ijk}(l,m)$ through which it filters the LGN ON and OFF cell input patterns $s^+(l,m)$ and $s^-(l,m)$. The dot products of these weight images and the LGN activity patterns are calculated to determine the bottom-up inputs I_i to the simple cells, scaled by the time-dependent decay function λ:

$$I_i(j,k)=\lambda(t)(w^+_{ijk}\cdot s^+_{jk}+w^-_{ijk}\cdot s^-_{jk}). \tag{9}$$

3.3. Simple cell dynamics

Each simple cell (or cell population) $x_i(j,k)$ obeys a membrane, or shunting, equation and combines bottom-up LGN input and recurrent positive feedback from the corresponding simple cell $y_i(j,k)$, as shown in Fig. 3. The recurrent excitation is multiplied by a habituating transmitter gate $z_i(j,k)$. In all:

$$\frac{dx_i}{dt}=-A_x x_i+(B_x-x_i)\{C_x I_i+E_x f[T(y_i)]z_i\} \tag{10}$$

with

$$T(y)=\begin{cases} y & \text{if } y>0,\\ 0 & \text{otherwise.}\end{cases} \tag{11}$$

Each simple cell (or cell population) $y_i(j,k)$ receives feedforward excitation from the corresponding simple cell $x_i(j,k)$ and inhibition from the competing simple cell $x_h(j,k)$. This recurrent local circuitry is functionally similar to the feedforward model of Shulz et al. (1993), and accounts for ON and OFF subregion inhibition (Hubel and Wiesel, 1962), opponency between paired simple cells (Liu et al., 1992; Palmer and Davis, 1981; Pollen and Ronner, 1981), and the survival of orientation tuning following blockade of activity in the ON afferents (Schiller, 1982). In addition, non-adaptive lateral connections provide short-range distance-dependent excitation and longer-range distance-dependent inhibition:

$$\frac{dy_i}{dt}=-A_y y_i+(B_y-y_i)\{C_y x_i+D_y\alpha_E G(\sigma_E)*f[T(y_i)]\}$$
$$-(y_i+F_y)\{E_y x_h+G_y\alpha_1 G(\sigma_1)*f[T(y_i)]\} \tag{12}$$

where opponent cells are designated by the index h:

$$h=\begin{cases} 0 & \text{if } i=1,\\ 1 & \text{if } i=0.\end{cases} \tag{13}$$

The signal function f in Eq. (12) is defined by:

$$f(y)=\frac{y^2}{f_1^2+y^2}. \tag{14}$$

Such sigmoidal signal functions enable the recurrent competitive field in Eq. (12) to achieve the useful properties of contrast enhancement and noise suppression (Grossberg, 1973), both of which are needed for pattern processing in a noisy environment. In the present case, within-channel excitatory connections and between-channel inhibitory connections cause the y cells to compute the difference of the cortical inputs, I_0 and I_1, to the two opponent channels. When weights w^+ and w^- are random, as they are before learning, these differences are very small and need to be amplified to enable cortical units to interact laterally with other cortical cells in such a way as to learn a map of

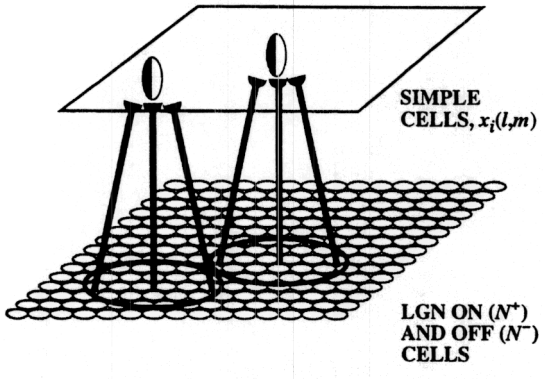

Fig. 2. LGN input organization: each simple cell $x_i(j,k)$ receives input from a circular region of LGN ON and OFF cells via weighted pathways. Indices j, k represent the position within the larger LGN images from which the input to the x units is taken.

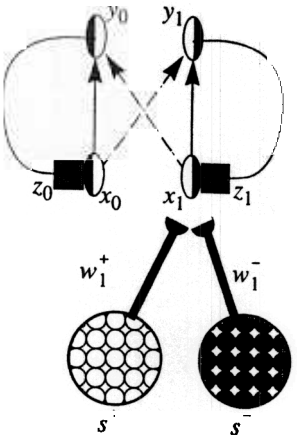

Fig. 3. Local connectivity: a single dipole unit is composed of a pair of input cells $x_i(j,k)$, feedback cells $y_i(j,k)$, and habituating gates $z_i(j,k)$ made up of two channels, corresponding to units with subscript 0 and to units with subscript 1, respectively. Each simple cell $x_i(j,k)$ receives LGN ON (+) and OFF (−) signals along weighted pathways. Vertical feedforward excitation (solid arrows) within and reciprocal feedforward inhibition (dashed arrows) between the channels produce an antagonistic relationship between simple cells. Positioned indices (j,k) have been dropped.

orientation and ocular dominance through weight changes (see below).

The $x \leftrightarrow y$ feedback loop amplifies such small input differences. This is accomplished through high-gain recurrent connections [with large values of C_y and E_x relative to the size of the input gain, C_x, in Eqs. (10) and (12)]. Similar feedback has been used in models of boundary segmentation (e.g. Gove et al., 1995) and has been reported in neural measurement of cortical neurons (Chung and Ferster, 1997; Douglas et al., 1995; Stratford et al., 1996). Once a pattern of activation is instantiated in the network by high-gain feedback, lower-gain subsequent inputs may be of insufficient magnitude to force the selection of a new pattern. To amplify input differences, the gain on the feedback loop needs to be large relative to the bottom-up input gain, but to respond efficiently to changing input patterns, the input gain must be large relative to the feedback gain.

3.4. Habituative or depressing synapses

This apparent paradox is resolved by adapting or habituating the feedback gain using a habituative transmitter, z_i, that gates the feedback signal as in Eq. (10). This transmitter obeys the equation:

$$\frac{dz_i}{dt} = A_z(1 - z_i) - B_z f[T(y_i)]z_i \tag{15}$$

(Grossberg, 1969, 1972). When the cell signal $f[T(y_i)]$ is zero, z_i gradually accumulates to a maximal value of 1 via the term $A_z(1 - z_i)$ in Eq. (15). However, when y_i is active, z_i is inactivated via the mass action term $B_z f[T(y_i)]z_i$ and reduces the effective gain on the $x \leftrightarrow y$ feedback loop. The time-dependent decay $\lambda(t)$ of input, as in Eq. (9), also alleviates the problem by allowing the effective input gain to be relatively large whenever a new input is presented. This sort of habituative synapse has been used to explain a variety of perceptual data that involve visual cortex (Francis, 1996a, b; Francis and Grossberg, 1996a, b; Francis et al., 1994; Grossberg, 1976b, 1980, 1987, 1997; Grunewald and Grossberg, 1996). Abbott et al. (1997) have reported habituating cells in rat visual cortex and modeled them using Eq. (15). Their model also represents individual spikes. They call the habituation synaptic depression. Chance et al. (1997) have used habituative synapses to simulate a number of temporal non-linearities in the experimentally reported responses of simple cells.

The medium-range excitatory connections and long-range inhibitory connections, shown in Fig. 4, produce medium-range correlations and long-range anti-correlations in the developing maps of orientation and ocular dominance. These patterns of correlation and anti-correlation lead to the formation of coordinated maps of ocular dominance and orientation (Durbin and Mitchison, 1990; Grossberg and Olson, 1994; Obermayer et al., 1990, 1992; Sirosh and Miikkulainen, 1994; Swindale, 1992).

3.5. Complex cell receptive field

The activities of the simple cells, y_i, of both contrast polarities, combine additively through non-adaptive distance-dependent Gaussian connections to yield complex cell responses:

$$K = \alpha_k[T(y_0) + T(y_1)] * G(\sigma_k). \tag{16}$$

The parameter α_k is chosen such that the volume under the surface of the Gaussian is equal to 1.0.

Because simple cells with complementary receptive field profiles are found at nearby positions in the final simple cell map, complex cells which sum these responses exhibit similar response profiles to light and dark stimuli. The

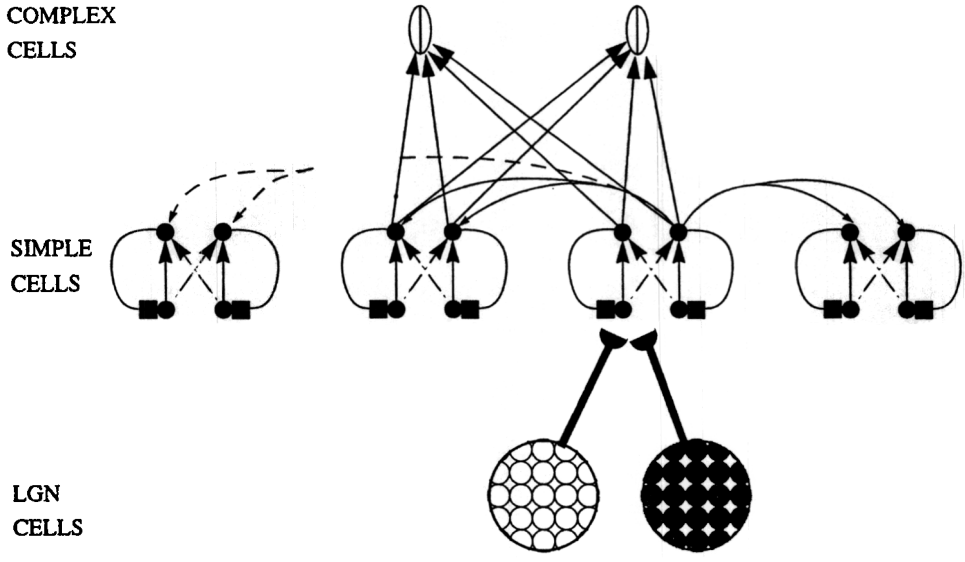

Fig. 4. Lateral connectivity and complex cells: distance-dependent connection strengths between y units realize a band pass filter. Complex cells respond according to the weighted sum of simple cell responses.

smoothness of a complex cell's response to light and dark stimuli in different positions in the receptive field may be controlled by varying the size of the region of the simple cell map that the complex cell samples. Small regions, corresponding to values of σ_k near 0, lead to segregated patches in the complex cell receptive field corresponding to ON and OFF subregions in the underlying simple cells. Large values of σ_k lead to a more uniform spatial response distribution within the receptive field.

For small values of σ_k, the orientation preference of complex cells echoes the orientation preference of simple cells directly below them. With larger values of σ_k, each complex cell samples a broader range of simple cells and hence a broader range of orientations. The organization of the simple cell orientation map, which ensures that nearby simple cells have similar orientation preference, reduces the loss of orientation tuning that such broad sampling would otherwise dictate. Only when the sampling region is on the same order as the periodicity of the orientation map, with $\sigma_k > 2\sigma_I$, would orientation tuning in the complex cells be compromised.

3.6. Learned modification of geniculocortical path weights

At the beginning of a learning simulation, each element in each of the weight arrays w_{ijk}^{+} and w_{ijk}^{-} in Eq. (9) is selected from a uniform random distribution between 0 and 0.1 (Press et al., 1992). Modification of receptive field properties over time is due to changes in the long-term weights on the bottom-up connections. These weights are modified according to the following associative learning rule (Hebb, 1949), called the instar learning rule or gated steepest descent learning rule (Grossberg, 1976a, b; see also Kohonen, 1989; Obermayer et al., 1992; Singer, 1983):

$$\frac{d}{dt}w_{ijk}^{+}(l,m) = A_w T[x_i(j,k) - \Gamma][s^{+}(j,k) - w_{ijk}^{+}(l,m)], \quad (17)$$

$$\frac{d}{dt}w_{ijk}^{-}(l,m) = A_w T[x_i(j,k) - \Gamma][s^{-}(j,k) - w_{ijk}^{-}(l,m)]. \quad (18)$$

According to this learning rule, changes in the weights are made only when the postsynaptic cortical unit $x_i(j,k)$ is active. Then the weights slowly change to track the input signals impinging on the corresponding pathways. The instar rule is thus the simplest rule that can incorporate both Hebbian and anti-Hebbian learning properties. The instar learning rule also normalizes the weights when activity in the presynaptic and postsynaptic neural fields is normalized by their shunting on-center off-surround dynamics, and renders the sum of the elements of each cortical unit's weight arrays approximately constant.

In order to observe map formation in the system described by Eqs. (1)–(18), a large number of simple cell dipoles must be simulated. Since the weights change slowly compared to the rate of change of the other variables of the system {guaranteed by a small value of the expression $A_w T[x_i(j,k)\text{-}\Gamma]$ in Eqs. (17) and (18)}, it is possible to use the following approximation scheme for each input cycle, c:

1. a new random LGN input image L^{+} is selected;
2. the weights are assumed to remain constant, and solutions for the remaining fast dynamical variables, $x_{ijk}(\tau_m)$, are numerically computed at several time intervals τ_0 through τ_n using an adaptive stepsize Runge–Kutta algorithm (Press et al., 1992)—the number of steps n and the size of each step is determined by the numerical integration algorithm;
3. the weights are updated, using discrete-time approximations to Eqs. (17) and (18) and the time-averaged numerical solutions, $\overline{x_{ijk}}(c)$, of each x_{ijk} for the duration of cycle c:

$$w_{ijk}^{+}(c+1) = w_{ijk}^{+}(c) + A_w \overline{x_{ijk}}(c)[s_{jk}^{+}(c) - w_{ijk}^{+}(c)]$$

and

$$w_{ijk}^{-}(c+1) = w_{ijk}^{-}(c) + A_w \overline{x_{ijk}}(c)[s_{jk}^{-}(c) - w_{ijk}^{-}(c)]$$

where

$$\overline{x_{ijk}}(c) = \frac{1}{\tau_n}\sum_{m=1}^{n} x_{ijk}(\tau_m)(\tau_m - \tau_{m-1}).$$

This singular perturbation procedure eliminates the need to evaluate the evolution of the weights at the fast time scale of the rest of the activation dynamics and greatly reduces the number of computations required at each cycle.

4. Model simulations of a triple-o self-organizing cortical map

To simulate map formation at the same cortical resolution presented by Miller (1994) requires 32 × 32 dipoles in the system, each with six elements (two xs, two ys, and two zs), for a total of 6144 elements. Numerically integrating a system of 6144 variables using an adaptive stepsize algorithm such as the Runge–Kutta method would be possible, but somewhat inconvenient, except for the fact that the system is stiff (Press et al., 1992). Algorithms such as adaptive-stepsize Runge–Kutta take tiny time steps in order to obtain acceptably accurate solutions. In practice, the Runge–Kutta algorithm takes on the order of 106 steps to compute a single cycle of the integration phase.

By comparison, algorithms designed for stiff systems can perform much better. However, available stiff algorithms use more sophisticated techniques for estimating the influence that changes in one dynamical variable have on another and require multiple inversions of the Jacobian matrix (a matrix of size $n \times n$ for a system with n variables). Each matrix inversion (in general) requires on the order of n^3 operations (which translates to 2.3×10^{11} operations in a system of 6144 variables) and the storage of n^2 matrix elements (which translates to about 3×10^8 elements or

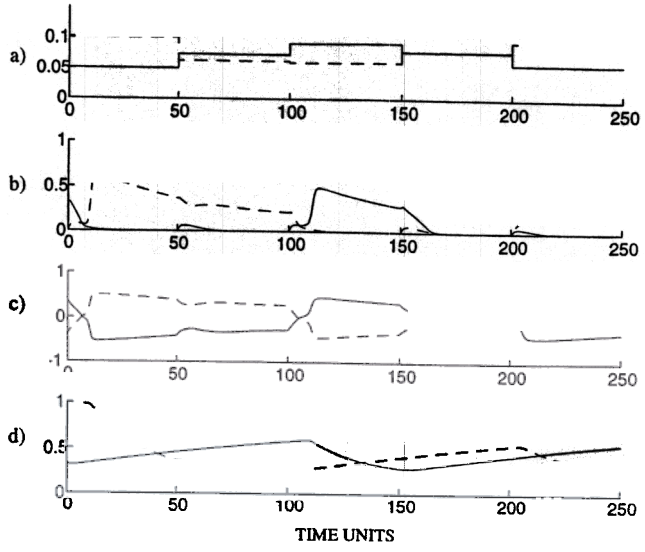

Fig. 5. Network dynamics: sample of five pulses used in weight modification procedure (see text). (a) Input pulses I_0 (solid) and I_1 (dashed) determined by Eqs. (1)–(9) with each element of L chosen randomly between 0 and 1. Solution traces of the variables comprising one dipole: (b) x_0 (solid) and x_1 (dashed); (c) y_0 (solid) and y_1 (dashed); (d) z_0 (solid) and z_1 (dashed). Parameters used were: $A_w = 0.002$, $A_x = 1$, $B_x = 1$, $C_x = 1$, $E_x = 6$, $A_y = 3$, $B_y = 1$, $C_y = 6$, $D_y = 1.5$, $E_y = 6$, $F_y = 1$, $G_y = 2$, $A_z = 0.005$, $B_z = 0.0444$, $n_1 = 16$, $n_2 = 32$, $f_1 = 0.3333$, $\sigma_i = 10$, $\sigma_E = 2.5$, $\sigma_I = 5$, $\sigma_1 = 2$, $\sigma_2 = 5$, $\alpha_E = 0.2257$, $\alpha_I = 0.1129$, $\alpha_1 = 0.0796$, $\alpha_2 = 0.0134$, $\beta = 0.2$, $\Gamma = 0.2$. These same parameters were used for all one-dimensional simulations shown. All simulations were run on an SGI Power Challenge using programs written in C, C++ and MatLab.

1152 megabytes of storage). Readily available computers cannot handle such large problems. Therefore, two approximations of the system are studied: a one-dimensional slice of the complete dynamical system in order to demonstrate how a map of orientation can develop, and a two-dimensional operational approximation (see Appendix A) to the complete dynamics that self-organizes ocular dominance and orientation maps with simple cell neighbors sensitive to opposite contrast polarities.

4.1. One-dimensional simulations: development of opponent simple cell orientation columns

Fig. 5 shows the responses through time of the variables that make up one opponent pair, or dipole, of simple cells. Every 50 time units, each element of the input image L^+ is selected from a uniform random distribution, representing spatially uncorrelated retinal activity. The presentation of a new input, which occurs every 50 time units, causes a small increase in the level of activity of the target simple cell x in Eq. (10), at a rate proportional to the total input. As activity in these x units increase, each y unit in Eq. (12) is excited by its corresponding x unit, and inhibited by the opponent x unit. Each y unit is thus sensitive to inputs to the corresponding x unit that are larger than those to the complementary x unit. As activity in the y units increases, a positive $x \leftrightarrow y$ feedback loop becomes active, driving the active x and y units towards their maximal levels and the opponent x and y units towards their minimal levels. The gradual decay of the transmitter z term in Eq. (15) of the active channel results in a decrease in the gain of the feedback loop and causes a gradual decay of activity in the active units. The decrease in feedback gain enables new inputs to drive the selection of other cortical units, notably the opponent simple cells.

These network dynamics are capable of robustly driving the learning of simple cell receptive field profiles. Since each x unit receives nearly complementary input images from the ON and OFF LGN cells according to Eqs. (5) and (6):

$$N^+ \cong 1 - N^-, \tag{22}$$

the total input to each input cell in Eq. (10) is approximately

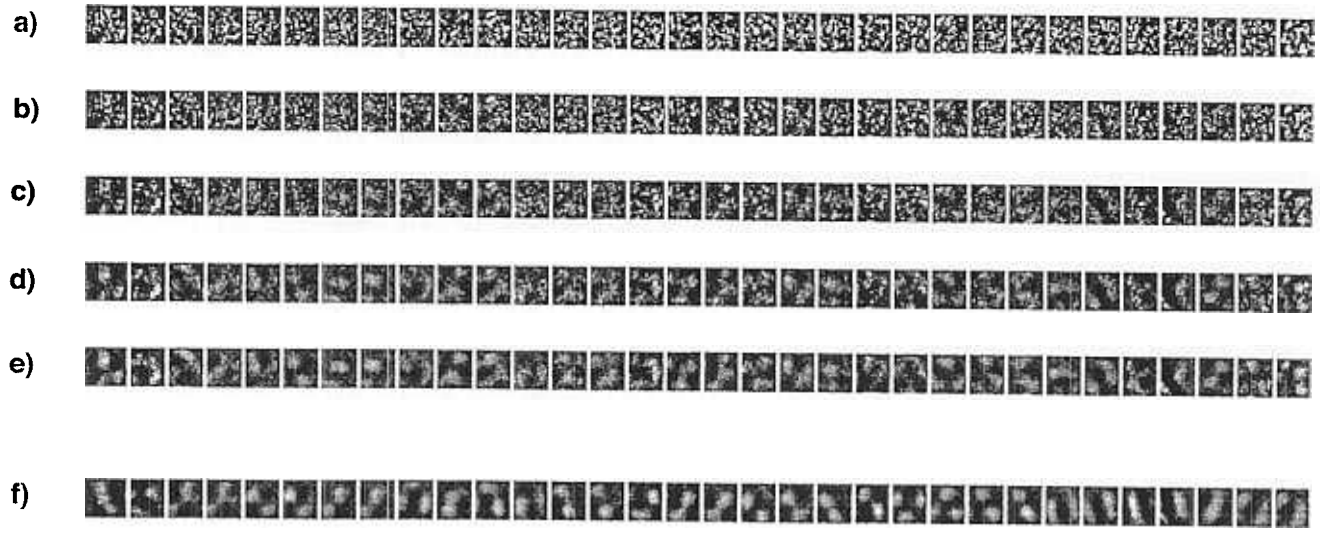

Fig. 6. Development of weight profiles: linearized weight images $\tilde{w}_{jk}$ corresponding to each of 32 cortical locations. Weight profiles gradually develop from initially disordered state and eventually converge to their final values. (a) Initial linearized weights; (b) after 250 training cycles; (c) after 500 presentations; (d) after 750; (e) after 1000; and (f) after 6000 presentations.

$$N^+[w_{ijk}^+ + (1 - w_{ijk}^-)], \tag{23}$$

which is a linear approximation of the feedforward component of the response of each simple cell x_{ijk} or y_{ijk}. Since the members of each pair compete subtractively with one another, the response of units y_0 is:

$$N^+\{[w_{0jk}^+ + (1 - w_{0jk}^-)] - [w_{1jk}^+ + (1 - w_{1jk}^-)]\}, \tag{24}$$

which simplifies to

$$N^+[(w_{0jk}^+ - w_{0jk}^-) - (w_{1jk}^+ - w_{1jk}^-)]. \tag{25}$$

The linearized weight image

$$\bar{w}_{jk}(l,m) = [w_{0jk}^+(l,m) - w_{0jk}^-(l,m)] - [w_{1jk}^+(l,m) - w_{1jk}^-(l,m)] \tag{26}$$

is thus a linear approximation of the feedforward component of the receptive field of each unit.

The gradual evolution of the linearized weight images is shown in Fig. 6. From their initially random state, the weight images are slowly transformed by associative learning into oriented, stable patterns. These weight profiles are similar to receptive field profiles of cortical simple cells. Furthermore, as shown in Fig. 6(f), nearby model simple cells tend to have similar orientation preferences, with orientation preference changing smoothly as the simulated cortex is traversed in a manner comparable to orientation preference of cells in the visual cortex along tangential electrode penetrations (Hubel and Wiesel, 1963).

A closer look at the weight images corresponding to a single opponent pair of simple cells (Fig. 7) reveals that, after development, model ON and OFF weight images corresponding to a single simple cells are complementary. This might be expected of any system capable of generating segregated ON and OFF subregions, but the fact that the ON weight images (as well as the OFF weight images) of opponent simple cells within a single dipole are complementary as well is an important result of this model. The mutual inhibitory connections from each x unit to the complementary y unit ensure that only one of the two positive $x \leftrightarrow y$ feedback loops in each dipole can become active at a time. Since the associative learning rule modifies the feedforward weights to make the response to subsequent presentations of the same pattern stronger, and since complementary x units respond in a statistically anti-correlated fashion, the corresponding weight images sample complementary input images and develop opposite spatial phases. Such complementary receptive field profiles have been recorded in vivo (Liu et al., 1992; Pollen and Ronner, 1981) from nearby cortical cells.

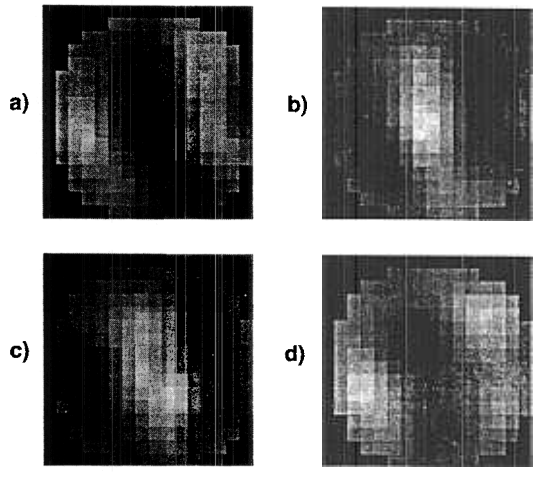

Fig. 7. Opponency of final weight profiles: self-organization leads to the development of opposite polarity ON and OFF weight profiles in opponent simple cells. Weight images after 6000 training presentations: (a) $w_0^+(1,24)$; (b) $w_0^-(1,24)$; (c) $w_1^+(1,24)$; (d) $w_1^-(1,24)$.

A second important result is that non-overlapping, oriented ON and OFF subregions develop in the model geniculocortical cell weights. Simple cells in the primary visual cortex receive direct excitatory connections from distinct regions of the LGN (Liu et al., 1992; Reid and Alonso, 1995). These distinct ON and OFF subregions provide direct oriented input to cortical simple cells (Ferster et al., 1996; Hawken and Parker, 1984; Reid and Alonso, 1995; Schiller, 1982). This model thus suggests how prenatal development leads to the segregation of initially intermingled ON and OFF inputs to cortical cells into oriented excitatory subregions.

4.2. Two-dimensional simulations: development of a triple-o map

In the two-dimensional model, the one-dimensional cortical slice simulated above is expanded to a two-dimensional sheet and the complete activity dynamics are simplified to obtain computational tractability (see Appendix A). This simplification permits a study of the interaction of orientation and ocular dominance map development. Each simple cell receives input from LGN fields corresponding to the contralateral (N^{C+} and N^{C-}) and the ipsilateral (N^{I+} and N^{I-}) eyes. These inputs converge onto simple cells via weighted pathways labeled w_{ijk}^{C+}, w_{ijk}^{C-}, w_{ijk}^{I+} and w_{ijk}^{I-}. As in the one-dimensional case, linearized weights are calculated in order to examine the response profiles of the cortical units. Linearized weight images corresponding to each eye are calculated, as in Eq. (26), by:

$$\bar{w}_{jk}^{C} = (w_{0jk}^{C+} - w_{0jk}^{C-}) - (w_{1jk}^{C+} - w_{1jk}^{C-}) \tag{27}$$

and

$$\bar{w}_{jk}^{I} = (w_{0jk}^{I+} - w_{0jk}^{I-}) - (w_{1jk}^{I+} - w_{1jk}^{I-}). \tag{28}$$

Linearized contralateral and ipsilateral weight images are shown in Figs. 8 and 9. Both possess regions with swirling patterns of oriented ON and OFF subregions. Interspersed with these are relatively neutral regions with little spatial ON/OFF discrimination. A comparison of the two figures reveals that the high contrast regions of the ipsilateral weights line up with the low contrast regions of the

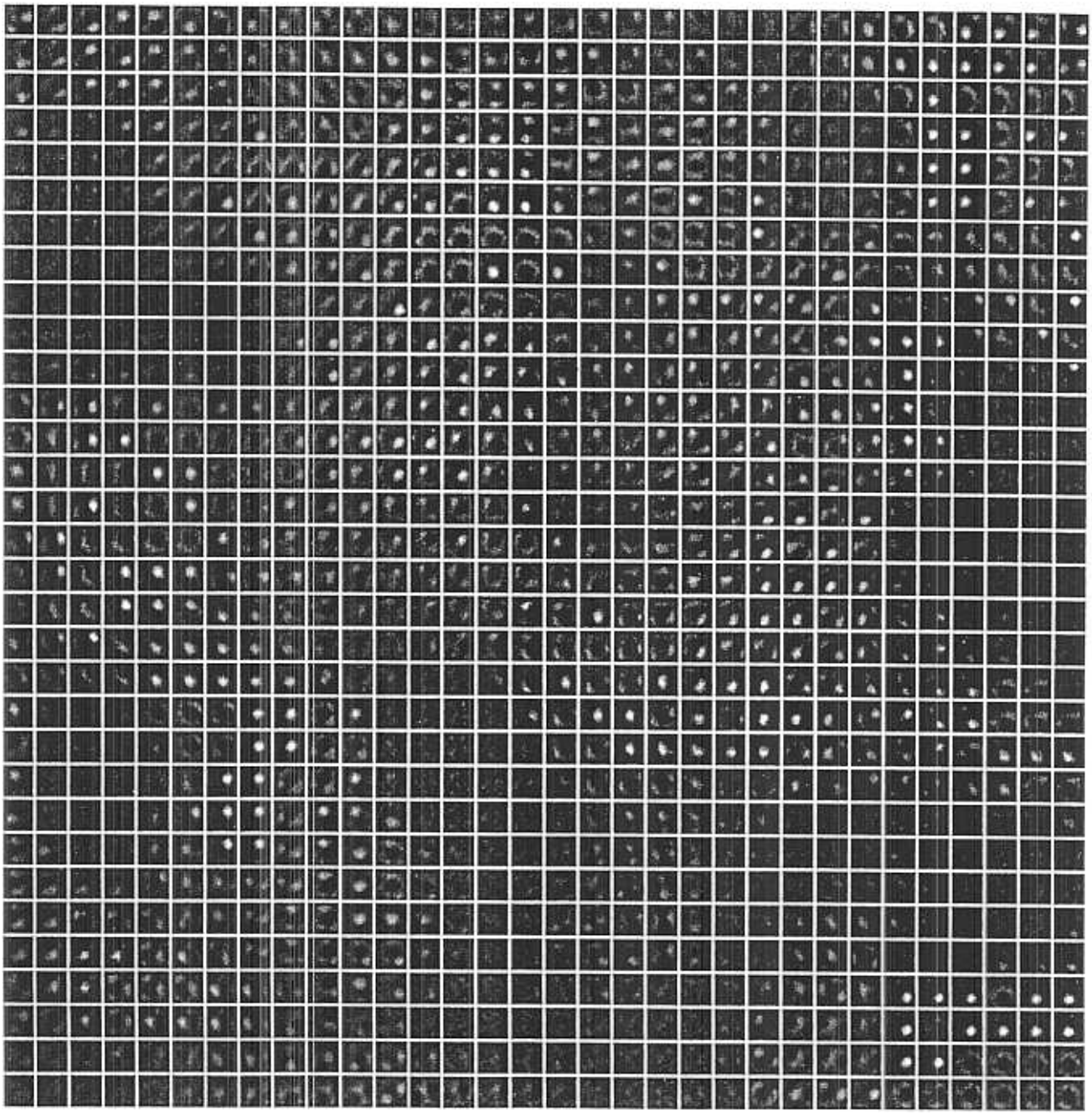

Fig. 8. Contralateral linearized weights: 24 × 24 subset of weight images $\bar{w}_{jk}^{C}$ after 10,000 learning iterations. Light areas represent regions with large ON weights to units x_{0jk} and dark areas represent regions with large OFF weights to these cortical units. Parameters used were: $A_w = 15$, $n_1 = 16$, $n_2 = 64$, $\sigma_E = 2$, $\sigma_I = 6$, $\sigma_1 = 2$, $\sigma_2 = 5$, $\sigma_k = 6$, $\alpha_E = 0.0796$, $\alpha_I = 0.0088$, $\alpha_1 = 0.0796$, $\alpha_2 = 0.0134$, $\alpha_E = 0.0088$, $\beta = 0.2$. These same parameters were used for all two-dimensional simulations shown.

contralateral weights, and visa versa. Each high contrast area in the contralateral weight image corresponds to a region dominated by the contralateral eye. In order to examine the global map of orientation independently of ocular dominance, binocular linearized weights are defined as:

$$\bar{w}_{jk}^{B} = \bar{w}_{jk}^{C} + \bar{w}_{jk}^{I}. \tag{29}$$

This is not to imply that the simple cells in the model are binocular. In fact it is because each simple cell is close to being monocular that ipsilateral and contralateral linearized weights may be meaningfully combined as in Eq. (29).

Linearized binocular weight images are shown in Fig. 10. As in the one-dimensional simulations, individual units develop oriented weight images that are strongly suggestive of the receptive field profiles of cortical simple cells. The gradual swirling arrangement of physiological orientation maps is also evident.

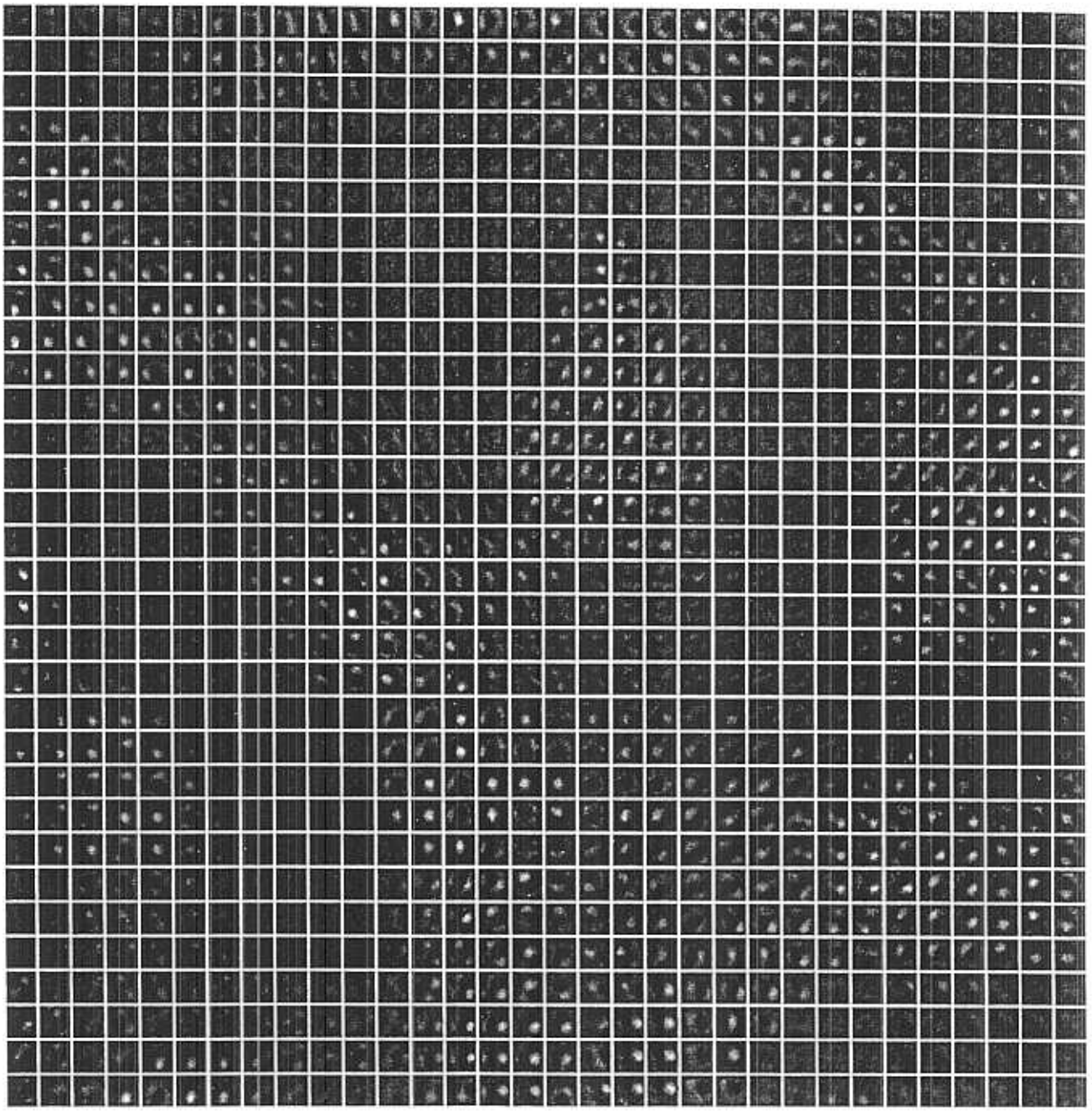

Fig. 9. Ipsilateral linearized weights: 24 × 24 subset of weight images $\vec{w}^{\mathrm{I}}_{jk}$.

To more closely examine these orientation preference maps, a quantitative measure of binocular orientation selectivity is computed directly from $\vec{w}^{\mathrm{B}}_{jk}$ by constructing a collection of images $B_{\theta ixy}$ of small (two pixel by eight pixel) light ($i = 1$) and dark ($i = 0$) bars on a neutral background (0.5) at 12 orientations θ, and every possible position (x,y) in a 16 × 16 grid. Responses to these test stimuli are then:

$$r^{\mathrm{B}}_{\theta}(j,k) = \sum_{i,x,y} B_{\theta ixy} \cdot \vec{w}^{\mathrm{B}}(j,k). \tag{30}$$

Following Blasdel (1992a), the responses at each cortical position to each orientation are vectorially summed to yield orientation preference

$$P^{\mathrm{B}}(j,k) = \frac{1}{2}\mathrm{atan}\left[\frac{\sum_{\theta} r^{\mathrm{B}}_{\theta}(j,k)\sin(2\theta)}{\sum_{\theta} r^{\mathrm{B}}_{\theta}(j,k)\cos(2\theta)}\right] \tag{31}$$

and orientation selectivity

$$S^{\mathrm{B}}(j,k) = \sqrt{\left[\sum_{\theta} r^{\mathrm{B}}_{\theta}(j,k)\sin(2\theta)\right]^2 + \left[\sum_{\theta} r^{\mathrm{B}}_{\theta}(j,k)\cos(2\theta)\right]^2}. \tag{32}$$

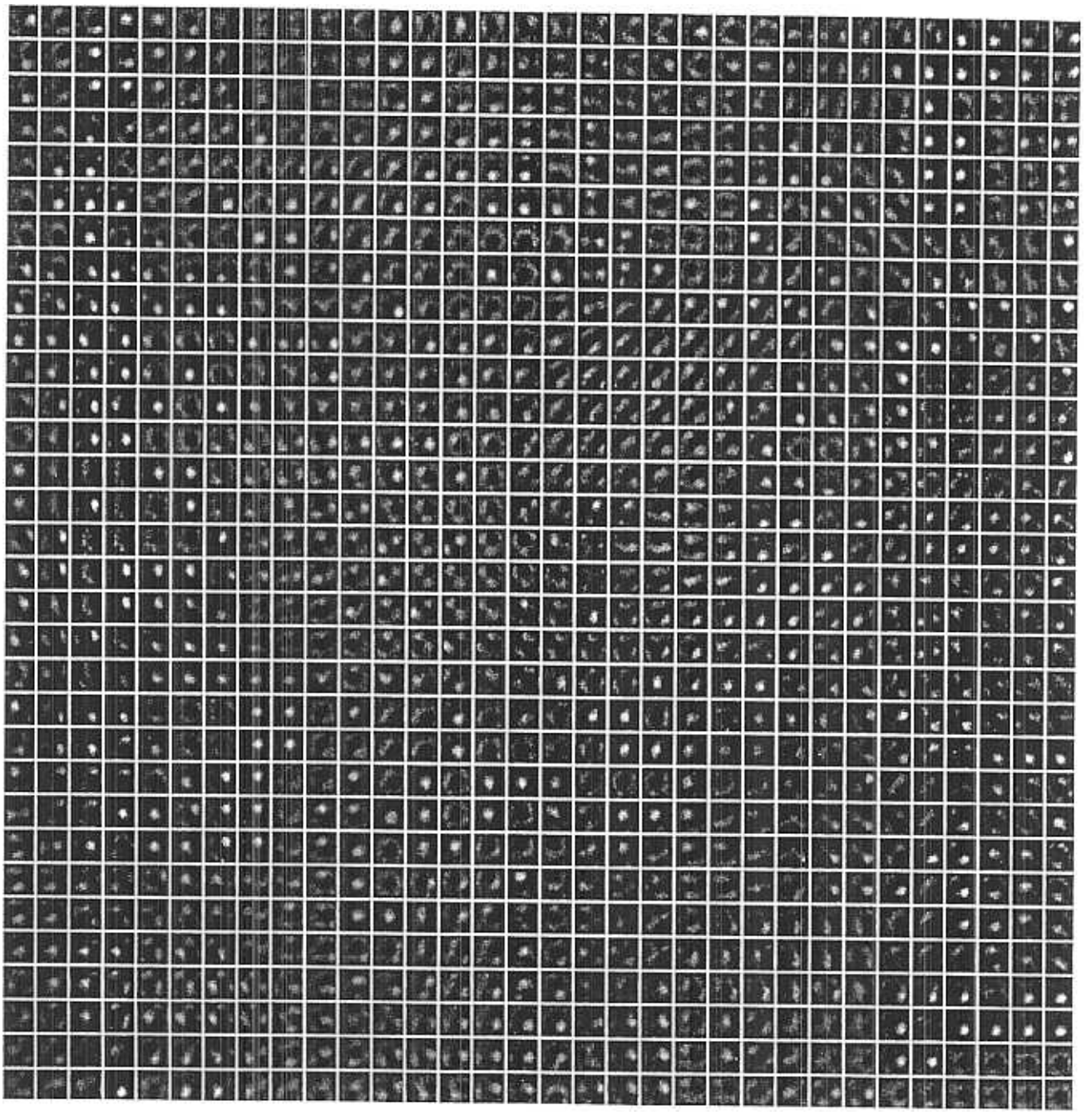

Fig. 10. Binocular linearized weights: 24 × 24 subset of weight images $\bar{w}^{B}_{jk}$.

Quantities P^{B} and S^{B} define a map of orientation that is shown in Fig. 11. At each position (j,k), a small line segment with orientation $P^{B}(j,k)$ and length proportional to $S^{B}(j,k)$ is drawn to represent orientation preference and selectivity. This map exhibits the swirling, gradually changing character of biological orientation maps as well as the key features of these maps: singularities—regions of low selectivity around which all other orientations are grouped, linear zones—regions in which orientation changes relatively linearly with cortical distance, and fractures—regions in which orientation changes rapidly along one spatial direction and slowly or not at all in the orthogonal direction. Each of these key features is present in the simulated orientation map shown in Fig. 11.

An index of ocular dominance is computed by subtracting the total weight contributed by the ipsilateral eye from the total weight contributed by the contralateral eye at each cortical position:

$$E(j,k)=\sum_{i,l,m}\{[w^{C+}_{ijk}(l,m)+w^{C-}_{ijk}(l,m)] - [w^{I+}_{ijk}(l,m)+w^{I-}_{ijk}(l,m)]\}. \quad (33)$$

Fig. 12 shows the complete orientation map superimposed

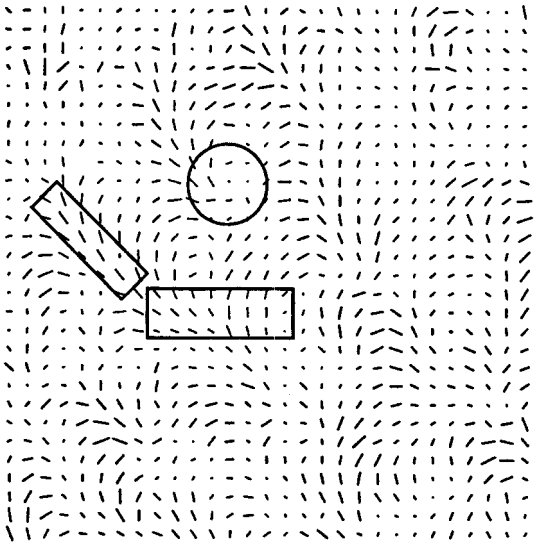

Fig. 11. Orientation map: subset of the simulated binocular orientation map. Key features of the biological orientation maps are present here: (a) singularities; (b) linear zones; (c) fractures.

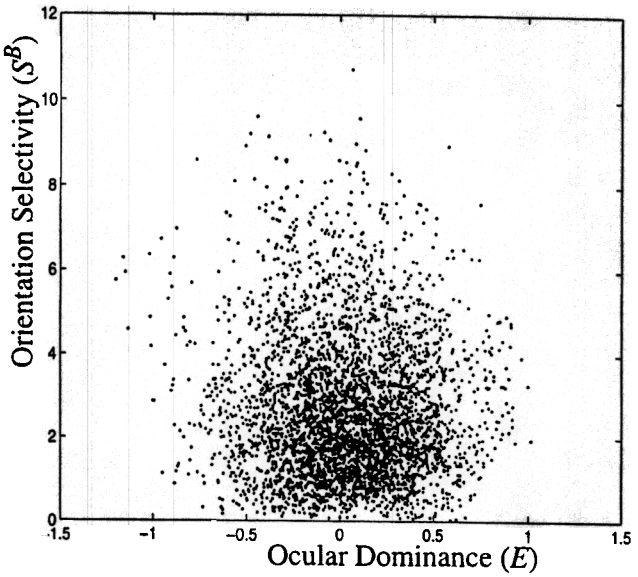

Fig. 13. Scatter plot of orientation selectivity vs. ocular dominance: the distribution reveals that large values of S^B tend to lie near cortical regions dominated by neither eye (E near 0), and that regions of extreme ocular dominance tend to have fairly low orientation selectivity.

on the map of ocular dominance. Regions dominated by the contralateral eye, with $E(j,k) \geq 0$, are colored white, and regions dominated by the ipsilateral eye, with $E(j,k) < 0$, are colored grey. As with physiological maps, this map of ocular dominance is made up of interlaced dark and light patches corresponding to regions dominated by each eye. Ocular dominance and orientation preference are related in much the same way as are physiological maps: regions dominated by one eye or the other (corresponding here to extreme values of E) tend to line up with regions of low orientation selectivity, and regions of high selectivity tend to be aligned with the borders of the ocular dominance bands (Blasdel, 1992b), as shown in Fig. 13. Earlier modeling work has shown that using an anisotropic filter can produce striped ocular dominance maps that even more closely resemble the patterns observed experimentally in monkeys (Grossberg and Olson, 1994; Rojer and Schwartz, 1989, 1990; Swindale, 1980). This could be accomplished within the present modeling framework either through the use of an anisotropic pattern of lateral connections among simple cells or through an anisotropic pattern of geniculocortical connectivity.

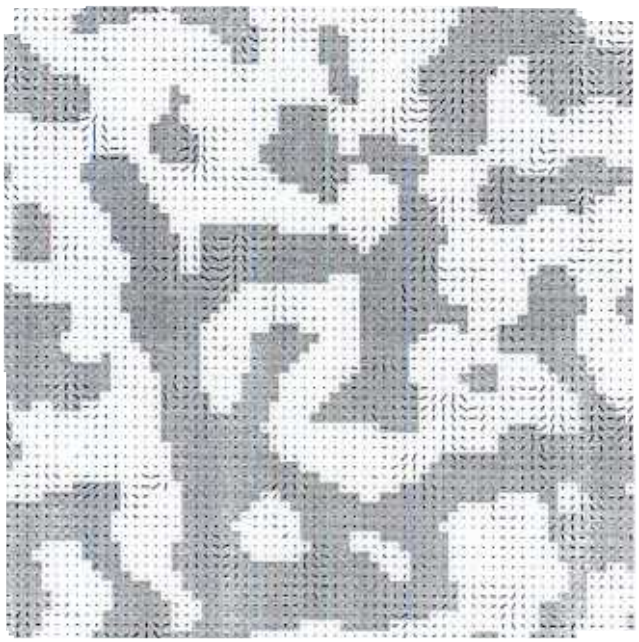

Fig. 12. Orientation preference and ocular dominance maps: orientation preference at each position is indicated by a line segment at the preferred orientation with length proportional to orientation selectivity. Regions dominated by the contralateral eye are colored white, regions dominated by the ipsilateral eye are grey.

The response properties of the simple and complex cells in the model are probed by constructing appropriate input images L^C and L^I, and computing the cortical response to each input using Eqs. (A1)–(A17) in Appendix A. Measuring the response of each cortical cell to oriented light (1.0) and dark (0.0) bars on a neutral (0.5) background in L^C and a uniform neutral pattern in L^I leads to the construction of contralateral orientation tuning curves for simple and complex cells. Figs. 14 and 15 show contralateral orientation tuning curves for six representative simple and complex cells, measured with oriented bars of length 12 and width 3. Similar response tuning curves result from presenting bars to the network in L^I, and uniform neutral stimuli in L^C. Both simple and complex cells tend to have a range of orientations for which they are well-tuned, and response falls off as the orientation is moved away from the preferred orientation. The orientation tuning of simple cells is approximately equal to that of complex cells.

In rhesus monkeys, most cells exhibit tuning curves

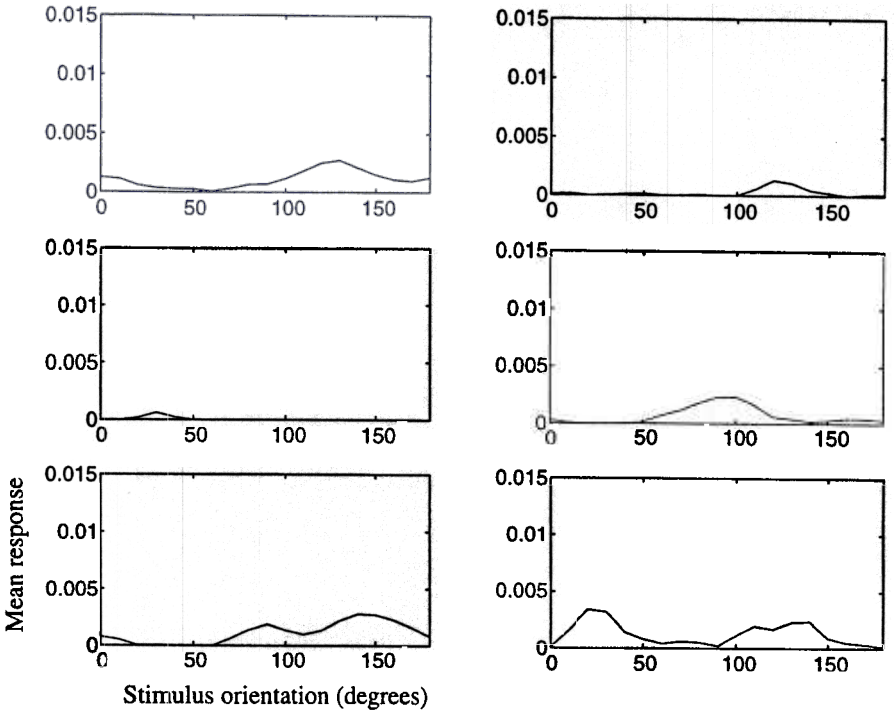

Fig. 14. Simple cell orientation tuning: model cell response plotted against test bar orientation for six characteristic model simple cells.

between 20 and 100 degrees wide, with the median at about 40 degrees for simple cells and 50–60 degrees for complex cells (Schiller et al., 1976) when orientation tuning was measured as the width of the tuning curve at a level equal to $1/\sqrt{2}$ of the maximum response. In cats it is between 40 and 75 degrees (median 50 degrees) for simple and between 20 and 81 degrees (median 47 degrees) for complex cells (Gilbert, 1977), when orientation tuning was measured as the width of the tuning curve at 1/2 the maximum response. Although direct comparison of these numbers is difficult because of the different definitions of tuning width, the measurements are in general agreement with one another and with the width of the tuning curves produced by the model.

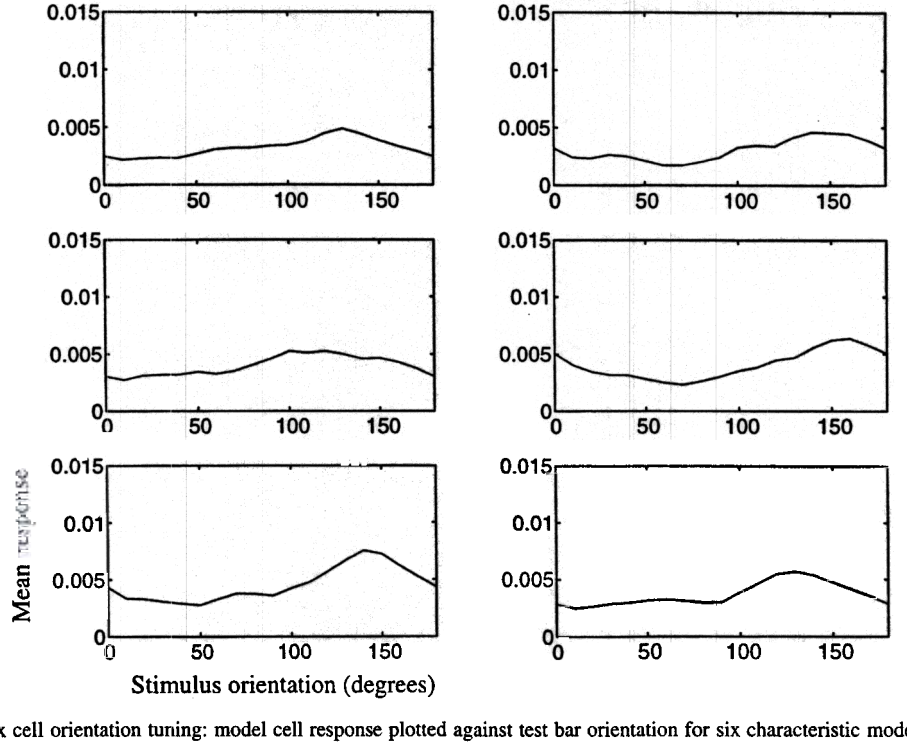

Fig. 15. Complex cell orientation tuning: model cell response plotted against test bar orientation for six characteristic model complex cells.

Model cells exhibit a range of orientation tuning, but most tend to exhibit tuning curves approximately 50 degrees wide (measured at a level equal to 1/2 the maximal response). A subset of simple cells exhibit bi-lobed orientation tuning curves with peaks in the orientation tuning curves at nearly orthogonal orientations. An example of this is shown in the lower right curve in Fig. 14 and is comparable to bi-lobed cells found in macaque visual cortexes (De Valois et al., 1982). Simple cell orientation tuning curves are also quite sensitive to bar position and contrast, a fact which is not surprising given the spatially distinct ON and OFF subregions they exhibit (see below). Because they pool inputs from many simple cells, the orientation tuning curves of complex cells are much less sensitive to stimulus position and contrast, and also tend to be broader and smoother than simple cell tuning curves.

ON and OFF regions of simple and complex cell receptive fields were probed using oriented bars at that orientation which produced the maximal response. Light and dark bars at the best orientation are presented at varying positions in each cell's receptive field in a path running orthogonal to the preferred orientation. Figs. 16 and 17 show the positional tuning curves of six representative simple and complex cells. Both model cell types show spatially localized receptive field profiles which tend to be aligned with the centers of the extent of their geniculate inputs. Like cortical simple cells, simple cells in the model have well-segregated ON and OFF subregions which lead to strong response when light and dark bars, respectively, are presented within the regions. These receptive field profiles possess multiple ON and OFF subregions reflecting both even-symmetric and odd-symmetric receptive field types. Some simple cells exhibit only ON responses (or conversely, only OFF responses), such as the cell shown in the center-right tuning curve of Fig. 16. Complex cells have poorly segregated ON and OFF subfields, often responding equally well to light and dark bars at each position in their receptive fields.

One of the novel aspects of the model is the development of spatially contiguous simple cells with opposite spatial phases or contrast polarities. These adjacent cortical simple cells provide input to a subsequent layer of complex cells, which thus pool signals from both contrast polarities. The fact that these opponent pairs of simple cells have receptive profiles which are anti-correlated implies that the ON weight profiles of paired simple cells become complementary (as do the OFF weight profiles of the paired cells). This fact, along with the fact that ON and OFF weight profiles corresponding to a single simple cell become complementary, implies that the ON weight profile of a simple cell becomes complementary to the OFF weight profile of the cell's antagonist. These tendencies are clearly evident in the scatter plots in Fig. 18.

5. Discussion

The self-organizing cortical map (SOCM) model developed in this study extends earlier work on map formation (Bienenstock et al., 1982; Grossberg, 1976a, c; Grossberg and Olson, 1994; Kohonen, 1989; Miller, 1992, 1994;

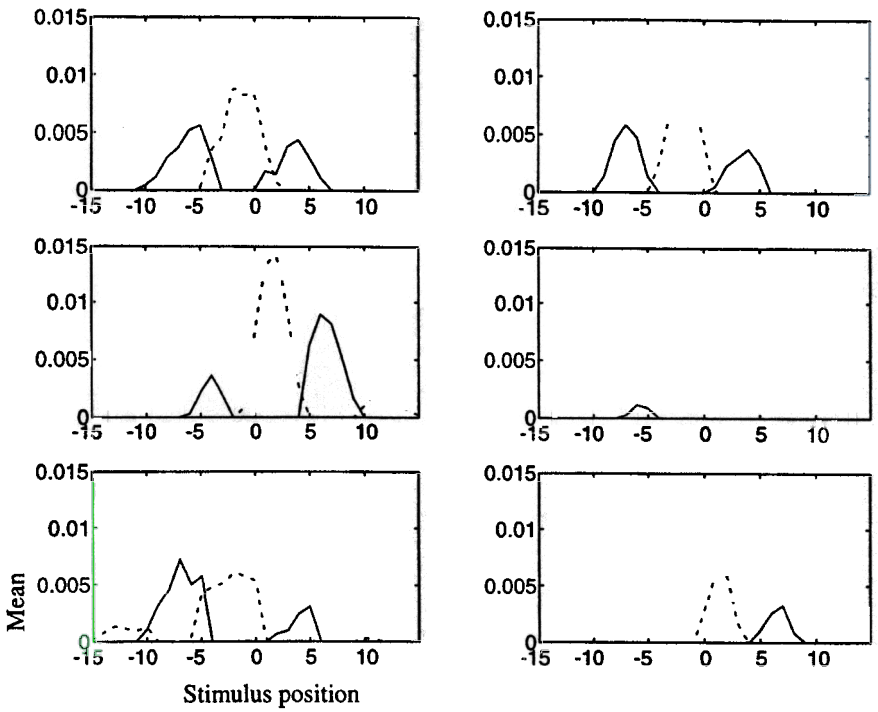

Fig. 16. Simple cell positional tuning: response elicited by bars at optimal orientation, averaged over position in receptive field (measured orthogonal to bar orientation). Position 0 corresponds to a stimulus centered in the portion of the LGN providing direct feedforward input to the simple cell. Solid lines: responses to light bars; dashed lines: responses to dark bars.

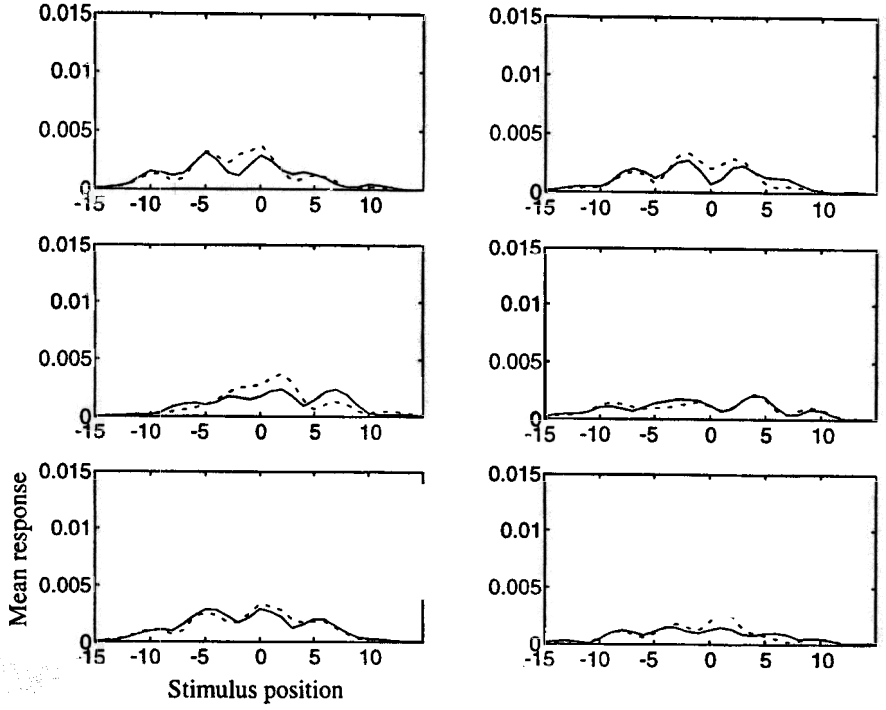

Fig. 17. Complex cell positional tuning: response elicited by bars at optimal orientation, averaged over position in receptive field (measured orthogonal to bar orientation). Solid lines: responses to light bars; dashed lines: responses to dark bars.

Miller et al., 1989; Rojer and Schwartz, 1989, 1990; Sirosh and Miikkulainen, 1994; von der Malsburg, 1973; Willshaw and von der Malsburg, 1976) and orientation tuning development (Linsker, 1986a, b, c; Miller, 1994) to show how neighboring simple cells that are sensitive to opposite contrast polarities can self-organize as part of the developmental process that generates cortical maps of orientation and ocular dominance. In addition to the source of noise, band pass filter, and response normalization that are present in other models, the current model makes use of cell dynamics to control map development. In contrast, the Miller (1994) model describes rules for learning neural connections without describing the dynamics of the cells between which these connections form. Using cell dynamics enables us to model how short-range inhibitory connections may lead to the generation of locally opponent simple cells with segregated ON and OFF subregions. These simple cell pairs interact via medium-range excitatory and long-range inhibitory connections that control the formation of cortical maps of orientation and ocular dominance. These several processes, acting together, enable the present SOCM model to show, for the first time, how triple-o map properties (orientation, ocular dominance, opponency) self-organize during the map development process. The fact that nearby simple cells develop opponent contrast polarities in the model allows, in turn, a simple description of complex cell self-organization to be proposed.

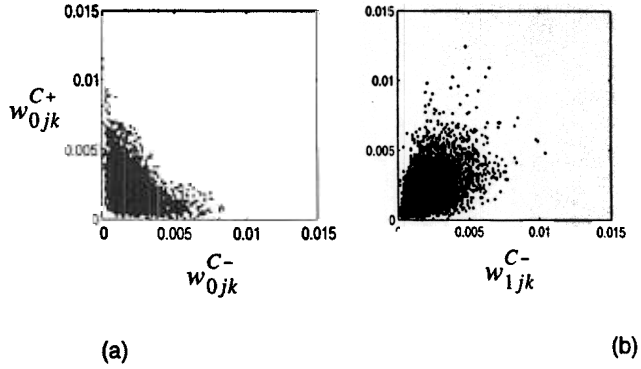

Fig. 18. Simple cell opponency: (a) value of each weight $w^{C+}_{0jk}(l,m)$ from the ON LGN to units x_{0jk} vs. weight $w^{C-}_{0jk}(l,m)$ from the OFF LGN. They are clearly anti-correlated. (b) Value of each weight $w^{C+}_{0jk}(l,m)$ from the ON LGN to units x_{0jk} vs. weight $w^{C-}_{1jk}(l,m)$ from the OFF LGN to the antagonistic units x_{1jk}. Because of the opponency developed by the model cells, each cell has an ON region that is correlated with the OFF region of its opponents.

Orientation tuning in the model is an emergent property of a network in which bottom-up random inputs to locally opponent simple cells drive high-gain local feedback and lateral on-center off-surround interactions between simple cells. There is strong evidence that, after development, cortical simple cells receive ON and OFF inputs via a well-oriented geniculocortical projection pattern (Ferster, 1986; Liu et al., 1992; Reid and Alonso, 1995; Volgushev et al., 1993). These inputs are arranged in alternating patches corresponding to the ON and OFF subregions of simple cell receptive fields (Ferster et al., 1996; Hawken and Parker, 1984; Schiller, 1982). Like earlier models of simple cell development (Linsker, 1986a, b, c; Miller, 1994), associative learning in model simple cell weights leads to this pattern of segregated ON and OFF inputs.

Orientation tuning can also be altered under appropriate

conditions by the blockade of the cortical inhibitory neurotransmitter GABA (Sillito, 1975, 1979; Vidyasagar and Mueller, 1994). These results suggest that intracortical connectivity can influence orientation tuning. In the model, the development of orientation tuning benefits from lateral inhibition within the cortical map, which serves to contrast enhance small differences in random activity before the map develops, along with well-oriented geniculocortical afferents. The apparently contradictory fact that application of the excitatory neurotransmitter acetylcholine does not lead to a decrease in orientation tuning, and may actually serve to enhance tuning (Sillito et al., 1985), may also be explained within the context of the model. General application of an excitatory transmitter would have the effect of increasing the level of activity in the x and y cells, tending to produce a shift in the balance of lateral excitation and inhibition. Compensating for the increased activity in y units would be a general increase in inhibition, which would tend to maintain a relatively constant level of mean cortical activity (Grossberg, 1976a, b). However, this increased level of excitation could also turn up the gain in the $x \leftrightarrow y$ feedback loop, resulting in substantially enhanced responses to preferred stimuli.

Intracellular blockade of inhibition has been found to have little effect on the orientation selectivity of cortical cells in vivo (Nelson et al., 1994). In the present model, orientation tuning is an emergent property of feedforward excitation and recurrent excitation and inhibition. Blocking the ability of a cell to respond to inhibitory inputs will thus not have a substantial impact on its orientation tuning. This conclusion is in accord with the model of Somers et al. (1995), which also suggests that orientation tuning arises through the interaction of feedforward excitation coupled with recurrent cortical excitation and 'iso-orientation' inhibition. After self-organization takes place in the present model (the Somers et al. model does not self-organize), nearby cortical cells exhibit similar orientation preference, and thus the medium-range connections provide tuned recurrent cortical excitation. Similarly the long-range inhibitory connections provide inputs from a broader spatial, and hence a broader orientation, range to make up the 'iso-orientation' inhibition described by Somers et al. (1995).

The complementary structure of the antiphase cells and the nature of local inhibition within each competitive pair leads to robust orientation selectivity in the model. Even when one population of geniculate inputs is deactivated, orientation tuning will remain. In vivo, the selective blockade of activity of ON ganglion cells (and hence the ON LGN cells to which they project) by the application of DL-2-amino-4-phosphonobutyric acid (APB) led to the elimination of light-edge responses in cortical simple cells, but had no effect on orientation selectivity (Schiller, 1982). In the model, removing the excitatory influence of ON cells from the x units would eliminate the responsiveness of the cells to bright bars within the normal ON region of the receptive fields, but the spatially-opponent OFF subregions in the two channels of each dipole would provide a receptive field of nearly unchanged shape.

The development of spatially contiguous simple cells that are sensitive to opposite contrast polarities clarifies how complex cells could develop by pooling signals from oppositely polarized simple cells. In fact, starting with pairs of such oppositely polarized simple cells, Grunewald and Grossberg (1996) have modeled how disparity-sensitive complex cell receptive fields can develop, despite the fact that the simple cells which activate them are anti-correlated. This study also uses habituative, or depressing, synapses to self-organize its receptive fields.

The pooling process whereby complex cells get their inputs from simple cells plays an important role in cortical models of visual perception. In these models, complex cells pool half-wave rectified output signals from pairs of oppositely polarized but similarly oriented simple cells. The model complex cells hereby compute an oriented, full-wave rectification of the image. Such an operation has become standard in models that have succeeded in explaining many data about human texture segregation (Chubb and Sperling, 1989; Grossberg and Mingolla, 1985b; Grossberg and Pessoa, 1997; Sutter et al., 1989). Because these model complex cells pool signals from opposite contrast polarities, they can respond all along the perimeter of objects whose relative contrast with respect to their backgrounds reverse along the perimeter. This property plays a key role in explaining many human psychophysical data about perceptual grouping, 3-D vision, and figure–ground separation (e.g. Francis and Grossberg, 1996a, b; Francis et al., 1994; Grossberg, 1994, 1997; Grossberg and Mingolla, 1985a, b). Taken together, these psychophysical and neurobiological data, and their explanation using complex cells that pool opponent simple cell outputs, provide strong converging evidence that simple cells provide an important input pathway to complex cells.

An ongoing debate concerns whether only simple cells project to complex cells (Hubel and Wiesel, 1968). The present model supports the hypothesis first presented by Hubel and Wiesel that orientation tuning in complex cells is initially derived from pooling the response of multiple simple cells. This hierarchical arrangement has been attacked based on several observations. Cross-correlation analysis of simple and complex cell action potentials seems to suggest that there exist relatively few direct simple to complex connections (Ghose et al., 1994; Hoffmann and Stone, 1971). If it is the case, as suggested by this model, that each complex cell pools the responses of many simple cells, firing of each simple cell may be only weakly correlated with firing in any complex cell. Although model simple to complex cell connections help to instantiate orientation tuning in model complex cells, the model is silent on the issue of whether additional oriented inputs reach complex cells. In vivo, complex cells may respond with shorter latencies via monosynaptic connections to

activity in LGN cells (Palmer and Davis, 1981; Tanaka, 1983, 1985), and two-dimensional visual noise displays, which are sufficient to drive complex cells, fail to drive simple cells (Hammond and MacKay, 1977). These observations suggest that complex cells receive a short-latency direct connection from LGN cells, but neither excludes the possibility that simple cells provide a major input to the complex cells.

Complex cells in layers 2 and 3 have been shown to have long-range connections to other superficial cells with similar preferred orientations (Gilbert and Wiesel, 1989). These connections spread evenly across large regions of the cortex shortly after birth, gradually coalesce, and eventually form the clustered patterns seen in the adult (Callaway and Katz, 1990). In accord with the need for correlated visual input to drive the final development of long-range connections, it has been shown that binocular deprivation leads to poor segregation of these developing connections (Callaway and Katz, 1991). In the model, as orientation tuning gets initiated due to prenatal amplification and smoothing of initial random biases in geniculocortical connections, activity-dependent processes could lead to initial clustering of long-range connections, and correlations present in the visual environment could subsequently produce long-range correlations in the map of complex cells, which could in turn drive associative learning of the adult pattern of long-range connections (Callaway and Katz, 1990). The model of Grossberg and Williamson (1997) begins to explore how such long-range connections develop both before eye opening and after visual inputs become effective.

Appendix A. Two-dimensional approximations

The number of dynamical variables in the system of differential equations described in the methods section precludes a two-dimensional study of orientation selectivity. Accordingly this dynamical system is approximated to yield an algorithm that is computationally tractable. With this approximation, it is also possible to include uncorrelated ON and OFF retinal inputs from the contralateral (C) and ipsilateral (I) eyes (L^{C+}, L^{C-}, L^{I+}, and L^{I-}) to investigate the joint development of orientation and ocular dominance maps.

The monocular Eqs. (5)–(9) are generalized in a straightforward way to construct LGN input images s_{jk}^{C+}, s_{jk}^{C-}, s_{jk}^{I+}, and s_{jk}^{I-} with segregated fields corresponding to contralateral and ipsilateral layers of the LGN:

$$N^{C+} = \frac{[\alpha_E G(\sigma_E) - \alpha_I G(\sigma_I)] * L^{C+}}{\beta + [\alpha_E G(\sigma_E) + \alpha_I G(\sigma_I)] * L^{C+}}, \tag{A1}$$

$$N^{C-} = \frac{[\alpha_E G(\sigma_E) - \alpha_I G(\sigma_I)] * L^{C-}}{\beta + [\alpha_E G(\sigma_E) + \alpha_I G(\sigma_I)] * L^{C-}}, \tag{A2}$$

$$N^{I+} = \frac{[\alpha_E G(\sigma_E) - \alpha_I G(\sigma_I)] * L^{I+}}{\beta + [\alpha_E G(\sigma_E) + \alpha_I G(\sigma_I)] * L^{I+}},$$

$$N^{I-} = \frac{[\alpha_E G(\sigma_E) - \alpha_I G(\sigma_I)] * L^{I-}}{\beta + [\alpha_E G(\sigma_E) + \alpha_I G(\sigma_I)] * L^{I-}}.$$

As shown in Fig. 2, each cortical cell $x_i(j,k)$ receives input signals $s^{C+}(j,k)$, $s^{C-}(j,k)$, $s^{I+}(j,k)$, and $s^{I-}(j,k)$ from circular regions of the LGN images shifted down and to the right with increasing values of j and k. The time-dependent component of Eq. (9) is removed to give

$$I_i(j,k) = w_{ijk}^{C+} \cdot s_{jk}^{C+} + w_{ijk}^{C-} \cdot s_{jk}^{C-} + w_{ijk}^{I+} \cdot s_{jk}^{I+} + w_{ijk}^{I-} \cdot s_{jk}^{I-}. \tag{A5}$$

The dynamical system is evaluated by first considering only the action of the feedforward inputs. Eqs. (10)–(15) are approximated by assuming a linear approximation to the activity in the x units (see Fig. 19):

$$x_i = \varepsilon I_i + y_i, \tag{A6}$$

which, when a new input is presented and is still negligible,

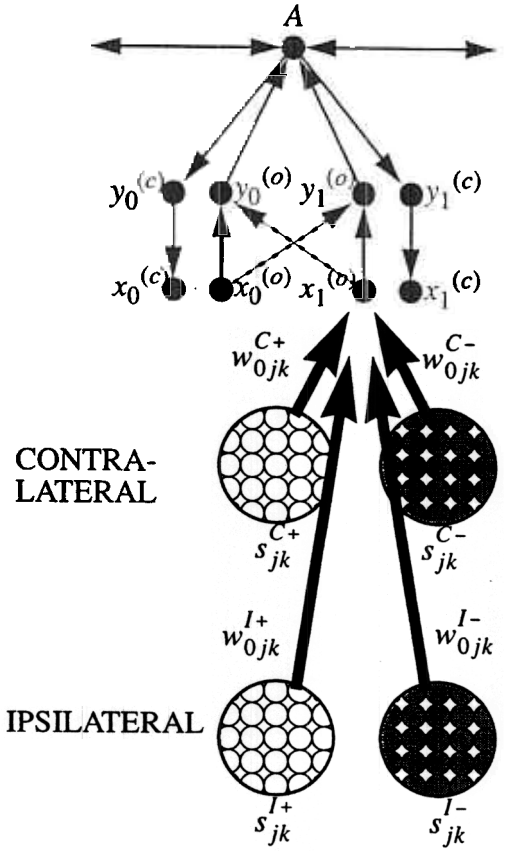

Fig. 19. Two-dimensional model: in addition to two cortical dimensions, inputs from both eyes are simulated. Contralateral (C) and ipsilateral (I) ON and OFF cells project via weighted retinotopically arranged pathways to each x unit. The two-dimensional model approximates the dynamical system as a progression of open (o) and closed loop (c) estimates.

becomes:

$$x_i^{(o)} \cong \varepsilon I_i, \tag{A7}$$

where the superscript (o) denotes 'open loop'. Because of the inhibitory connections from opponent x cells, only one $x \leftrightarrow y$ feedback loop at each position, the one receiving the larger total input, can become active at any time. Activity in the y units is driven by the thresholded difference between opponent channel activity values scaled by the input gains. The total lateral cortical feedback, A, also contributes to each y unit that is part of an active feedback loop:

$$y_0 = \varepsilon T(I_0 - I_1) + T(A)H(I_0 - I_1), \tag{A8}$$

$$y_1 = \varepsilon T(I_1 - I_0) + T(A)H(I_1 - I_0) \tag{A9}$$

where H is the Heaviside function

$$H(x) = \begin{cases} 0 & \text{if } x \leq 0, \\ 1 & \text{otherwise} \end{cases} \tag{A10}$$

Eqs. (A8) and (A9) lead to expressions for the open loop (o) y activity:

$$y_0^{(o)} = \varepsilon T(I_0 - I_1) \tag{A11}$$

and

$$y_1^{(o)} = \varepsilon T(I_1 - I_0) \tag{A12}$$

when the feedforward term dominates, as it does whenever a new input is presented. The lateral feedback interactions (A) are approximated as a convolution of the total feedforward activation with a difference of Gaussians; see Eq. (12). Thus:

$$A = [\alpha_E G(\sigma_E) - \alpha_I G(\sigma_I)] * (y_0^{(o)} + y_1^{(o)}). \tag{A13}$$

Terms A in Eq. (A13) are used to calculate the closed loop y values, denoted by $y^{(c)}$, when the A term dominates the ε term:

$$y_0^{(c)} = T(A)H(I_0 - I_1) \tag{A14}$$

and

$$y_1^{(c)} = T(A)H(I_1 - I_0). \tag{A15}$$

The final closed loop activity in the x units is then, by Eq. (A6):

$$x_i^{(c)} \cong y_i^{(c)}. \tag{A16}$$

The activities of the simple cells, $y_i^{(c)}$, combine additively through distance-dependent Gaussian connections to yield complex cell responses:

$$K = \alpha_k (y_0^{(c)} + y_1^{(c)}) * G(\sigma_k). \tag{A17}$$

As in the dynamical system, LGN-to-simple cell weights are modified according to an instar learning rule:

$$w_{ijk}^{C+}(t+1) = w_{ijk}^{C+}(t) + A_w x_{ijk}^{(c)}(t)[s_{jk}^{C+}(t) - w_{ijk}^{C+}(t)], \tag{A18}$$

$$w_{ijk}^{C-}(t+1) = w_{ijk}^{C-}(t) + A_w x_{ijk}^{(c)}(t)[s_{jk}^{C-}(t) - w_{ijk}^{C-}(t)], \tag{A19}$$

$$w_{ijk}^{I+}(t+1) = w_{ijk}^{I+}(t) + A_w x_{ijk}^{(c)}(t)[s_{jk}^{I+}(t) - w_{ijk}^{I+}(t)], \tag{A20}$$

$$w_{ijk}^{I-}(t+1) = w_{ijk}^{I-}(t) + A_w x_{ijk}^{(c)}(t)[s_{jk}^{I-}(t) - w_{ijk}^{I-}(t)]. \tag{A21}$$

References

Abbott, L. F., Varela, K., Sen, K., & Nelson, S. B. (1997). Synaptic depression and cortical gain control. *Science, 275*, 220–223.

Anderson, P., Olavarria, J., & Sluyters, R. (1988). The overall pattern of ocular dominance bands in cat visual cortex. *Journal of Neuroscience, 8*, 2183–2200.

Bienenstock, Cooper, & Munro (1982). Theory for the development of neuronal selectivity, Orientation specificity and binocular interaction in visual cortex. *Journal of Neuroscience, 2*, 32–48.

Blasdel, G. G. (1992a). Differential imaging of ocular dominance and orientation selectivity in monkey striate cortex. Journal of Neuroscience, 12(8), 3115–3138.

Blasdel, G. G. (1992b). Orientation selectivity, preference, and continuity in monkey striate cortex. Journal of Neuroscience, 12(8), 3139–3161.

Blasdel, G., & Salama, G. (1986). Voltage sensitive dyes reveal a modular organization in monkey striate cortex. *Nature, 321*, 579–585.

Bonhoeffer, T., & Grinvald, A. (1991). Iso-orientation domains in cat visual cortex are arranged in pinwheel-like patterns. *Nature, 353*, 429–431.

Callaway, E. M., & Katz, L. C. (1990). Emergence and refinement of clustered horizontal connections in cat striate cortex. *Journal of Neuroscience, 10 (4)*, 1134–1153.

Callaway, E. M., & Katz, L. C. (1991). Effects of binocular deprivation on the development of clustered horizontal connections in cat striate cortex. *Proceedings of the National Academy of Sciences, USA, 88*, 745–749.

Chance, F. S., Nelson, S. B., & Abbott, L. F. (1997). Effects of synaptic depression on temporal nonlinearities in response of model simple cells. *Society for Neuroscience Abstracts, 23*(II), 499.11, 1266.

Chung, S., & Ferster, D. (1997). The size of thalamic input to simple cells of the cat visual cortex. *Society for Neuroscience Abstracts, 23*(II), 801.7, 2059.

Chubb, C., & Sperling, G. (1989). Two motion perception mechanisms revealed through distance-driven reversal of apparent motion. *Proceedings of the National Academy of Sciences, USA, 86*, 2985–2989.

Cleland, B. G., Dubin, M. W., & Levick, W. R. (1971). Sustained and transient neurons in the cat's retina and lateral geniculate nucleus. *Journal of Physiology, 217*, 473–496.

De Valois, R. L., Yund, E. W., & Hepler, N. (1982). The orientation and direction selectivity of cells in macaque visual cortex. *Vision Research, 22*, 531–541.

DeAngelis, G. C., Ohzawa, I., & Freeman, R. D. (1991). Depth is encoded in the visual cortex by a specialized receptive field structure. *Nature, 352*, 156–159.

DeAngelis, G. C., Ohzawa, I., & Freeman, R. D. (1993). Spatiotemporal organization of simple cell receptive fields in the cat's striate cortex. I. General characteristics and postnatal development. *Journal of Neurophysiology, 69 (4)*, 1091–1117.

Douglas, R. J., Koch, C., Mahowald, M., Martin, K. A. C., & Suarez, H. H. (1995). Recurrent excitation in neocortical cells. *Science, 269*, 980–985.

Durbin, R., & Mitchison, G. (1990). A dimension reduction framework for understanding cortical maps. *Nature, 343*, 644–647.

Emerson, R. C., Korenberg, M. J., & Citron, M. C. (1992). Identification of complex-cell intensive nonlinearities in a cascade model of cat visual cortex. *Biological Cybernetics, 66*, 291–300.

Ferster, D. (1986). Orientation selectivity of synaptic potentials in neurons of cat primary visual cortex. *Journal of Neuroscience, 6*, 1284–1301.

Ferster, D., Chung, S., & Wheat, H. (1996). Orientation selectivity of thalamic input to simple cells of cat visual cortex. *Nature, 380*, 249–252.

Francis, G. (1996a). Cortical dynamics of lateral inhibition. Visual persistence and ISI. *Perception and Psychophysics, 58*, 1103–1109.

Francis, G. (1996b). Cortical dynamics of visual persistence and temporal integration. *Perception and Psychophysics, 58*, 1203–1212.

Francis, G., Grossberg, S. (1996a). Cortical dynamics of form and motion integration. Persistence, apparent motion and illusory contours. *Vision Research, 35*(25), 149–173.

Francis, G., & Grossberg, S. (1996b). Cortical dynamics of boundary segmentation and reset. Persistence, after-images, and residual traces. *Perception, 25*, 543–567.

Francis, G., Grossberg, S., & Mingolla, E. (1994). Cortical dynamics of feature binding and reset, control of visual persistence. *Vision Research, 34*, 1089–1104.

Ghose, G. M., Freeman, R. D., & Ohzawa, I. (1994). Local intracortical connections in the cat's visual cortex. Postnatal development and plasticity. *Journal of Neurophysiology, 72 (3)*, 1290–1303.

Gilbert, C. D. (1977). Laminar differences in receptive field properties of cells in cat primary visual cortex. *Journal of Physiology, 268*, 391–421.

Gilbert, C. D., & Wiesel, T. (1989). Columnar specificity of intrinsic horizontal and corticocortical connections in cat visual cortex. *Journal of Neuroscience, 9 (7)*, 2432–2442.

Gove, A., Grossberg, S., & Mingolla, E. (1995). Brightness perception, illusory contours, and corticogeniculate feedback. *Visual Neuroscience, 12*, 1027–1052.

Grinvald, A., Lieke, E. E., Frostig, R. D., & Hildesheim, R. (1994). Cortical point-spread function and long-range lateral interactions revealed by real-time optical imaging of macaque monkey primary visual cortex. *Journal of Neuroscience, 14 (5)*, 2545–2568.

Grossberg, S. (1969). On the production and release of chemical transmitters and related topics in cellular control. *Journal of Theoretical Biology, 22*, 325–364.

Grossberg, S. (1972). A neural theory of punishment and avoidance. II. Quantitative theory. *Mathematical Biosciences, 15*, 39–67.

Grossberg, S. (1973). Contour enhancement, short-term memory and constancies in reverberating neural networks. *Studies in Applied Mathematics, 52*, 217–257.

Grossberg, S. (1976a). Adaptive pattern classification and universal recoding. I. Parallel development and coding of neural feature detectors. *Biological Cybernetics, 23*, 121–134.

Grossberg, S. (1976b). Adaptive pattern classification and universal recoding. II. Feedback, expectation, olfaction, and illusions. *Biological Cybernetics, 23*, 187–202.

Grossberg, S. (1976c). On the development of feature detectors in the visual cortex with application to learning and reaction–diffusion systems. *Biological Cybernetics, 21*, 145–159.

Grossberg, S. (1980). How does a brain build a cognitive code? *Psychological Review, 1*, 1–51.

Grossberg, S. (1987). Cortical dynamics of three-dimensional form, color, and brightness perception. II. Binocular theory. *Perception and Psychophysics, 41*, 117–158.

Grossberg, S. (1994). 3-D vision and figure–ground separation by visual cortex. *Perception and Psychophysics, 55*, 48–120.

Grossberg, S. (1997). Cortical dynamics of 3-D figure–ground perception of 2-D pictures. *Psychological Review, 104*, 618–658.

Grossberg, S., & Mingolla, E. (1985a). Neural dynamics of form perception. Boundary completion, illusory figures, and neon color spreading. *Psychological Review, 92*, 173–211.

Grossberg, S., & Mingolla, E. (1985b). Neural dynamics of perceptual grouping, textures, boundaries, and emergent segmentations. *Perception and Psychophysics, 38*, 141–171.

Grossberg, S., & Olson, S. (1994). Rules for the cortical map of ocular dominance and orientation columns. *Neural Networks, 7 (6/7)*, 883–894.

Grossberg, S., & Pessoa, L. (1997). Texture segregation, surface representation, and figure ground separation. Technical Report CAS/CNS-TR-96-025, Boston University, Boston, MA. *Vision Research* (in press).

Grossberg, S., & Williamson, J. R. (1997). Linking cortical development to visual perception. *Society for Neuroscience Abstracts, 23*(I), 227.9, 568.

Grunewald, A., & Grossberg, S. (1996). Self-organization of binocular disparity tuning by reciprocal corticogeniculate interactions. Technical Report CAS/CNS-TR-96-027, Boston University, Boston, MA. *Journal of Cognitive Neuroscience* (in press).

Hammond, P., & MacKay, D. M. (1977). Differential responsiveness of simple and complex cells in cat striate cortex to visual texture. *Experimental Brain Research, 30*, 275–296.

Hawken, M. J., & Parker, A. J. (1984). Contrast sensitivity and orientation selectivity in lamina IV of the striate cortex of old world monkeys. *Experimental Brain Research, 54*, 367–372.

Hebb, D. E. (1949). *The organization of behavior*. Wiley, New York.

Hodgkin, A. L., & Huxley, A. F. (1952). A quantitative description of membrane current and its applications to conduction and excitation in the nerve. *Journal of Physiology, 117*, 500–544.

Hoffmann, K. P., & Stone, J. (1971). Conduction velocity of afferents to cat visual cortex. A correlation with cortical receptive field properties. *Brain Research, 42*, 146–157.

Horton, J. C., & Hocking, D. R. (1996). An adult-like pattern of ocular dominance columns in striate cortex of newborn monkeys prior to visual experience. *Journal of Neuroscience, 16 (5)*, 1791–1807.

Hubel, D. H., & Wiesel, T. N. (1962). Receptive fields, binocular interaction and functional architecture in the cat's visual cortex. *Journal of Physiology, 160*, 106–154.

Hubel, D. H., & Wiesel, T. N. (1963). Shape and arrangement of columns in cat's striate cortex. *Journal of Physiology, 165*, 106–154.

Hubel, D. H., & Wiesel, T. N. (1968). Receptive fields and functional architecture of monkey striate cortex. *Journal of Physiology, 195*, 215–243.

Hubel, D. H., & Wiesel, T. N. (1974). Sequence regularity and geometry of orientation columns in the monkey striate cortex. *Journal of Comparative Neurology, 158*, 267–293.

Hubel, D. H., Wiesel, T. N., & LeVay, S. (1977). Plasticity of ocular dominance columns in monkey striate cortex. *Philosophical Transactions of the Royal Society of London, Series B, 278*, 131–163.

Hubel, D. H., Wiesel, T. N., & Stryker, M. (1978). Anatomical demonstration of orientation columns in macaque monkey. *Journal of Comparative Neurology, 177*, 361–380.

Jacobson, L. D., Gaska, J. P., Chen, H.-W., & Pollen, D. A. (1993). Structural testing of multi-input linear–nonlinear cascade models for cells in macaque striate cortex. *Vision Research, 33 (5/6)*, 609–626.

Kohonen, T. (1982). Self-organized formation of topologically correct feature maps. *Biological Cybernetics, 43*, 59–69.

Kohonen, T., 1989. Self-Organization and Associative Memory, 3rd edn. Springer-Verlag, Berlin.

LeVay, S., Hubel, D., & Wiesel, T. (1975). The pattern of ocular dominance columns in macaque visual cortex revealed by a reduced silver stain. *Journal of Comparative Neurology, 159*, 559–576.

LeVay, S., Stryker, M., & Shatz, C. (1978). Ocular dominance columns and their development in layer IV of the cat's visual cortex, a quantitative study. *Journal of Comparative Neurology, 179*, 223–244.

LeVay, S., Connolly, M., Houde, J., & Van Essen, D. (1985). The complete pattern of ocular dominance stripes in the striate cortex and visual field of the macaque monkey. *Journal of Neuroscience, 5*, 486–501.

Linsker, R. (1986a). From basic network principles to neural architecture. Emergence of spatial-opponent cells. *Proceedings of the National Academy of Sciences, 83*, 7508–7512.

Linsker, R. (1986b). From basic network principles to neural architecture. Emergence of orientation-selective cells. *Proceedings of the National Academy of Sciences, 83*, 8390–8394.

Linsker, R. (1986c). From basic network principles to neural architecture. Emergence of orientation columns. *Proceedings of the National Academy of Sciences, 83*, 8779–8783.

Liu, Z., Gaska, J. P., Jacobson, L. D., & Pollen, D. A. (1992). Interneuronal interaction between members of quadrature phase and anti-phase pairs in the cat's visual cortex. *Vision Research, 32 (7)*, 1193–1198.

Löwel, S., Bischof, H., Leutenecker, B., & Singer, W. (1988). Topographic relations between ocular dominance and orientation columns in the cat striate cortex. *Experimental Brain Research, 71*, 33–46.

Löwel, S., & Singer, W. (1987). The pattern of ocular dominance columns in flat mounts of the cat visual cortex. *Experimental Brain Research, 68*, 661–666.

Miller, K. D. (1992). Development of orientation columns via competition between on- and off-center inputs. *NeuroReport, 3 (1)*, 73–76.

Miller, K. D. (1994). A model for the development of simple cell receptive fields and the ordered arrangement of orientation columns through activity-dependent competition between ON- and OFF-center inputs. *Journal of Neuroscience, 14 (1)*, 409–441.

Miller, K. D., Keller, J. B., & Stryker, M. P. (1989). Ocular dominance column development. Analysis and simulation. *Science, 245*, 605–615.

Nelson, S. B., Toth, L. J., Sheth, B., & Sur, M. (1994). Orientation selectivity of cortical neurons persists during intracellular blockade of inhibition. *Science, 265*, 774–777.

Obermayer, K., & Blasdel, G. G. (1993). Geometry of orientation and ocular dominance columns in monkey striate cortex. *Journal of Neuroscience, 13 (10)*, 4114–4129.

Obermayer, K., Ritter, H., & Schulten, K. (1990). A principle for the formation of the spatial structure of retinotopic maps, orientation and ocular dominance columns. *Proceedings of the National Academy of Sciences USA, 87*, 8345–8349.

Obermayer, K., Blasdel, G. G., & Schulten, K. (1992). Statistical–mechanical analysis of self-organization and pattern formation during the development of visual maps. *Physical Review A, 45 (10)*, 7568–7589.

Olson, S. J., & Grossberg, S. (1996). Self-organization of simple and complex cell cortical maps. *Investigative Ophthalmology and Visual Science Abstracts, 37*(3), S1073, #4930.

Palmer, L. A., & Davis, T. L. (1981). Receptive field structure in cat striate cortex. *Journal of Neurophysiology, 46 (2)*, 260–276.

Pollen, D. A., & Ronner, S. F. (1981). Phase relationships between adjacent simple cells in the visual cortex. *Science, 212*, 1409–1411.

Press, W. H., Teukolsky, S. A., Vetterling, W. T., & Flannery, B. P. (1992). *Numerical recipes in C*, 2nd edn. Cambridge University Press, Cambridge.

Reid, R. C., & Alonso, J.-M. (1995). Specificity of monosynaptic connections from thalamus to visual cortex. *Nature, 378*, 281–284.

Rojer, A. S., & Schwartz, E. L. (1989). A parametric model for synthesis of cortical column patterns. In International Joint Conference on Neural Networks, Vol. 2, p. 603.

Rojer, A., & Schwartz, E. (1990). Cat and monkey cortical columnar patterns modeled by band-pass-filtered 2d white noise. *Biological Cybernetics, 62*, 381–391.

Schiller, P. H. (1982). Central connections on the retinal ON- and OFF-pathways. *Nature, 297*, 580–583.

Schiller, P. (1992). The on and off channels of the visual system. *Trends in Neuroscience, 15*, 86–92.

Schiller, P. H., Finlay, B. L., & Volman, S. F. (1976). Quantitative studies of single-cell properties in monkey striate cortex. II. Orientation specificity and ocular dominance. *Journal of Neurophysiology, 39 (6)*, 1320–1333.

Shulz, D., Debanne, D., & Frégnac, Y. (1993). Cortical convergence of on- and off-pathways and functional adaptation of receptive field organization in cat area 17. *Progress in Brain Research, 95*, 191–205.

Sillito, A. M. (1975). The contribution of inhibitory mechanisms to the receptive field properties of neurons in the striate cortex of the cat. *Journal of Physiology, 250*, 305–329.

Sillito, A. M. (1979). Inhibitory mechanisms influencing complex cell orientation selectivity and their modification at high resting discharge levels. *Journal of Physiology*, 33–53.

Sillito, A. M., Salt, T. E., & Kemp, J. A. (1985). Modulatory and inhibitory processes in the visual cortex. *Vision Research, 25 (3)*, 375–381.

Singer, W. (1983). Neuronal activity as a shaping factor in the self-organization of neuron assemblies. In E. Basar, H. Flohr, H. Haken, A.J. Mandell (Eds.), *Synergetics of the brain*, pp. 89–101. Springer-Verlag, New York.

Sirosh, J., & Miikkulainen, R. (1994). Cooperative self-organization of afferent and lateral connections in cortical maps. *Biological Cybernetics, 71 (1)*, 66–78.

Somers, D. C., Nelson, S. B., & Sur, M. (1995). An emergent model of orientation selectivity in cat visual cortical simple cells. *Journal of Neuroscience, 15 (8)*, 5448–5465.

Spitzer, H., & Hochstein, S. (1985). A complex-cell receptive-field model. *Journal of Neurophysiology, 53 (5)*, 1266–1286.

Stratford, K. J., Tarcy-Hornoch, D., Martin, K. A. C., Bannister, N. J., & Jack, J. J. B. (1996). Excitatory synaptic inputs to spiny stellate cells in cat visual cortex. *Nature, 382*, 258–261.

Stryker, M. P., & Harris, W. (1986). Binocular impulse blockade prevents the formation of ocular dominance columns in cat visual cortex. *Journal of Neuroscience, 6*, 2117–2133.

Sutter, A., Beck, J., & Graham, N. (1989). Contrast and spatial variables in texture segregation, testing a simple spatial-frequency channels model. *Perception and Psychophysics, 46*, 312–332.

Swindale, N. (1980). A model for the formation of ocular dominance column stripes. *Proceedings of the Royal Society of London, Series B, 208*, 243–264.

Swindale, N. (1982). A model for the formation of orientation columns. *Proceedings of the Royal Society of London, Series B, 215*, 211–230.

Swindale, N. (1992). A model for the coordinated development of columnar systems in primate striate cortex. *Biological Cybernetics, 66*, 217–230.

Tanaka, K. (1983). Cross-correlation analysis of geniculostriate neuronal relationships in cats. *Journal of Neurophysiology, 49 (6)*, 1303–1318.

Tanaka, K. (1985). Organization of geniculate inputs to visual cortical cells in the cat. *Vision Research, 25 (3)*, 357–364.

Vidyasagar, T. R., & Mueller, A. (1994). function of GABAa inhibition in specifying spatial frequency and orientation selectivities in cat striate cortex. *Experimental Brain Research, 98*, 31–38.

Volgushev, M., Pei, X., Vidyasagar, T. R., & Creutzfeldt, O. D. (1993). Excitation and inhibition in orientation selectivity of cat visual cortex neurons revealed by whole-cell recordings in vivo. *Visual Neuroscience, 10 (6)*, 1151–1155.

von der Malsburg, C. (1973). Self-organization of orientation sensitive cells in the striata cortex. *Kybernetik, 14*, 85–100.

Willshaw, D., & von der Malsburg, C. (1976). How patterned neural connections can be set up by self-organization. *Proceedings of the Royal Society of London, Series B, 194*, 431–445